Case Studies in Construction Materials 22 (2025) e04723

Contents lists available at ScienceDirect

Case Studies in Construction Materials

journal homepage: www.elsevier.com/locate/cscm

Case study

Characterization of the effects of waste mullite powder on seawater sea sand cementitious materials

Xiao Sun [a], Zehui Zhou [a,*], Wenjie He [a], Yudong Bi [a], Yao Wang [a], Hengrui Liu [b], Rui Zhong [c], Hongyan Ma [c]

[a] College of Water Conservancy and Hydropower Engineering, Hohai University, Xikang Road No.1, Nanjing, Jiangsu 210098, China
[b] Department of Civil and Environmental Engineering, The Hong Kong Polytechnic University, Hung Hom, Kowloon, Hong Kong
[c] Department of Civil, Architectural and Environmental Engineering, Missouri University of Science and Technology, Rolla, MO 65401, USA

ARTICLE INFO

Keywords:
Seawater sea sand concrete
Waste mullite powder
Rapid Iodide migration
Durability

ABSTRACT

Maintaining the durability of coastal concrete structures while reducing construction costs remains a formidable challenge. Drawing inspiration from the volcanic concrete used by ancient Greeks and Romans, this study explores the feasibility of using waste mullite powder (WMP) with a high alumina content in seawater sea sand concrete to conserve natural resources and enhance durability. The experimental results demonstrate that the incorporation of seawater and WMP exerts detrimental impacts on the flow characteristics and workability of cementitious composites. While the sulfate content in seawater and sea sand can bolster the early strength of sea sand seawater concrete, sulfate attack compromises its long-term strength. Incorporating a small amount of WMP (3 %, 5 %) proved beneficial for compressive strength. To assess the chloride penetration resistance of SSC, the Rapid Iodide Migration test indicated that the alumina in WMP can adsorb and immobilize chloride ions. Microstructure characterizations show that the incorporation of WMP resulting in an increased content of calcium silicate hydrate gel and Friedel's salt in the hydration products. The observed modification substantially augments both the physicochemical binding mechanisms within the cementitious matrix, facilitating improved chloride ion immobilization through synergistic physical entrapment and chemical fixation processes.

1. Introduction

In the previous few decades, mainland China and other developing nations have seen a sharp increase in their consumption of concrete [1]. The mixture of concrete requires a large amount of freshwater and river sand. However, the freshwater resources available for industrial utilization are becoming increasingly scarce, and over 50 % of the global population will face water shortage by 2025 [2]. Excessive exploitation of river sand also has caused serious ecological and environmental problems. In addition, the imbalance between supply and demand of river sand has led to its price skyrockets. Therefore, freshwater and river sand are considered to be the two most valuable commodities in the 21st century [3]. The sea sand seawater concrete (SSC) prepared by replacing freshwater with seawater as concrete mixing water and sea sand instead of river sand is considered to be a new type of sustainable eco-friendly concrete [4], which can not only alleviate the problem of resource shortage to a certain extent, but also be conducive to

* Corresponding author.
E-mail address: 241602010089@hhu.edu.cn (Z. Zhou).

https://doi.org/10.1016/j.cscm.2025.e04723
Received 17 February 2025; Received in revised form 13 April 2025; Accepted 30 April 2025
Available online 2 May 2025

green construction in coastal and island areas, and has broad application prospects. Recent studies have demonstrated that seawater sea sand engineered geopolymer composites, as a novel construction material, not only achieve synergistic optimization of both high strength (exceeding 140 MPa) and high ductility (approximately 8 %), but also significantly reduce the reliance on natural resources by utilizing seawater and sea sand. This technological advancement offers a promising direction for sustainable development of marine engineering materials [5].

Researchers have explored various properties of SSC. Studies on the impact of seawater and sea sand on concrete workability have revealed that using seawater instead of freshwater reduces the setting time of concrete [6–8]. Compared to fresh water concrete, the slump of seawater concrete is reduced by approximately 20 % at the same water-to-cement ratio (w/c) [9]. The diminished workability of sea sand concrete relative to ordinary concrete primarily stems from the shell content in the sea sand. Specifically, concrete becomes less workable as the amount of shell in the sea sand rises [10–12].

SSC exhibited higher early compressive strength [13–15], though findings on its long-term strength varied across different studies. Mohammed et al. [16] posited that the inorganic salt ions in seawater could accelerate early hydration, thus enhancing the concrete's initial strength. They did point out, though, that the concrete's long-term strength development was negatively impacted by the subsequent salt crystal formation. Jau et al. [17] observed that the compressive strength of sea sand concrete peaked at 21 weeks, then declined by approximately 5 %-8 % by the 35th week. In contrast, Li et al. [18] found that SSC outperformed concrete made with freshwater and sand in terms of both early and late strengths. According to research by Yang et al. [19] and Alan et al. [20] found that increases in shell content in sea sand up to a certain level led to a decrease in both the compressive strength and elastic modulus of SSC as shell content increased.

The effects of seawater and sea sand on the durability of concrete primarily involve the corrosion resistance to chloride ions and sulfates, carbonation resistance, and freeze-thaw durability. Regarding permeability, Thaulow et al. [21] demonstrated that corrosive salt ions (Cl^-, SO_4^{2-}, etc.) crystallize within the pores, diminishing the durability of concrete. Xiao et al. [22] performed electric flux tests on concrete made from sea sand, desalinated sea sand, and river sand. They found that sea sand concrete exhibited the highest permeability. Zhen et al. [23] observed that the trend in carbonation depth for sea sand concrete mirrored that of river sand concrete, with carbonation depth increasing over time and with lower concrete strength grades. Yamato et al. [24] reported that freeze-thaw resistance declined when the chloride content in concrete exceeded 0.5 % of the cement weight. Thus, chloride and shell content are the primary factors limiting the broader application of SSC.

The misuse of sea sand can potentially damage or even cause the collapse of building structures, posing significant safety risks. In order to offset the influence of chloride on the durability of reinforced concrete structures, several nations have used "purification and desalination" techniques to guarantee that the performance of SSC satisfies technical standards. However, these methods are costly and inefficient in terms of desalination. It is mainly affected by high energy consumption, membrane contamination, complexity of pre-treatment, concentrated brine discharge problems and limitations of technology adaptability. Compared to freshwater treatment, desalination has an energy consumption of 3–25 kWh/m^3 due to osmotic pressure problems caused by high salinity (~35 ‰), far exceeding the 0.3–1 kWh/m^3 of freshwater treatment [25]. An alternative approach involves enhancing the internal structure of concrete and its capacity to bind chloride ions by incorporating suitable amounts of mineral admixtures, thereby improving SSC's overall performance. Zhu et al. [26] demonstrated that FRP-reinforced ultra-high-strength engineered cementitious composite panels can enhance the ultimate load-carrying capacity by 139 %–173 % while maintaining superior crack resistance, even when incorporating seawater, compared to conventional concrete systems. This synergistic effect not only mitigates chloride-induced corrosion but also facilitates sustainable construction in marine environments. Ramachandran et al. [27] demonstrated that concrete samples mixed with fly ash and a water-reducing agent in a seawater environment exhibited robust compressive strength and durability in ion penetration and carbonation tests. Li et al. [28] explored alkali-activated slag concrete mixed with seawater and sea sand, finding that concrete's chloride ion permeability resistance significantly improved with slag powder content between 15 % and 40 %, and compressive strength increased with higher slag content. Shi et al. [29] found that incorporating metakaolin in seawater concrete addressed the diffusion of free chloride ions by forming Friedel's salt, thus enhancing the concrete's resistance to chloride ion erosion. Although various materials have been investigated to enhance SSC's performance, further research is necessary to understand the improvement effects and mechanisms of these materials and to explore more sustainable options for enhancing SSC.

Recent analyses by experts on the main components of ancient Roman concrete have identified calcium aluminosilicate hydrate (C-A-S-H) gel as a key factor in its exceptional anti-corrosion performance. The incorporation of the aluminum phase facilitates the transformation of calcium silicate hydrate (C-S-H) gel into C-A-S-H gel, enhancing its ability to bind chloride ions as more aluminum phase substances infiltrate. This has drawn significant attention to the role of the aluminum phase in improving concrete durability [30]. Myers et al. [31] analyzed the crystal structure of C-A-S-H gel and discovered its structural similarity to the tobermorite mineral group. Mullite, an aluminosilicate mineral, is the only stable crystalline compound in the SiO_2-Al_2O_3 binary system under atmospheric pressure, characterized by a high content of aluminum in its structure. Mullite is a significant synthetic refractory material, with low-grade waste mullite powder (WMP) being a byproduct of its production. Inspired by ancient Roman concrete, WMP is proposed as an admixture in this study to assess its potential enhancements or impacts on SSC's performance. This study examines the impact of WMP on the rheological properties of seawater cement paste (SCP), analyses of the rheological and mechanical properties of sea sand seawater mortar (SSM), as well as macroscopic mechanical testing and durability assessments of SSC.

2. Materials and test methods

2.1. Materials

The test water was categorized into freshwater and seawater. The chemical composition of freshwater is primarily dominated by H_2O, with only trace amounts of dissolved ions such as Ca^{2+}, Mg^{2+}, Na^+, and K^+. The total dissolved solids (TDS) typically remain below 500 mg/L. In contrast, seawater used in this study was prepared by dissolving instant sea salt crystals, yielding a chemical composition closely resembling that of natural seawater. It contains high concentrations of Na^+ (~10.8 g/kg) and Cl^- (~19.4 g/kg), along with significant levels of Mg^{2+} (~1.3 g/kg), SO_4^{2-} (~2.7 g/kg), Ca^{2+} (~0.4 g/kg), and K^+ (~0.4 g/kg). Additionally, minor components such as HCO_3^- and Br^- are also present, forming a complex multivalent electrolyte system. The salinity of the seawater was measured using a high-precision seawater salinity meter. The salinity of the simulated seawater used in this experiment was set consistently at 35 ‰. The primary compositions and indices of the cement used in the tests (P.O. 42.5), are listed in Table 1 and Table 2.

Table 2 and Fig. 1 show the WMP's primary chemical compositions and particle size distribution, respectively. The predominant component of WMP is Al_2O_3, with lower concentrations of SiO_2 and CaO. The combined content of SiO_2, Al_2O_3, and Fe_2O_3 in WMP totals approximately 90.43 %, thus meeting the requirements to be used as mineral admixtures in concrete and cement-based materials. Particle size analysis shows that 90 % of WMP particles are smaller than 72.2 μm, predominantly ranging between 20 and 70 μm.

The test sand was composed of sea sand and ISO standard sand from the Guangxi region of Beihai, China. Fig. 2 shows the samples of sand. The Chinese Standard "Sand for building" GB/T 14684–2022 [32] was used to evaluate the primary characteristics of these sand samples. Table 3 lists the relevant parameters that were discovered during these testing. Table 4 shows the grading proportion for the coarse aggregate, which was constantly graded crushed stone ranging from 5 mm to 25 mm. The water reduction agent uses a superplasticizer made of PCA-I polycarboxylic acid.

2.2. Mixture proportion

There were three stages to the test plan. Studying the rheological characteristics of cement paste by adjusting the mixing water, w/c, and WMP content was the main goal of the first phase. The fluidity and mechanical characteristics of mortars made with regular sand and sea sand were compared in the second phase using tests for compressive strength and fluidity. Additionally, the impact of varying WMP content on the properties of these two mortars was assessed. Through a battery of tests, the third phase examined and assessed how WMP affected the workability and longevity of SSC, including the slump test, sulfate resistance test under wet-dry cycling conditions, chloride ion electric flux test, and Rapid Iodide Migration (RIM) test.

The w/c chosen for this test in the study's initial phase were 0.3, 0.4, 0.5, and 0.6. The amount of WMP added ranged from 0 %, 3 %, 5 %, and 10 % of the cement dosage to examine how the WMP content affects the cement paste's rheological properties. WMP replacement levels of 3 %, 5 %, and 10 % were selected to systematically evaluate their effects on the rheological properties, mechanical strength, and durability of cementitious materials. Preliminary experimental results indicated that the 3–5 % range offered an optimal balance between performance and cost. While higher replacement level, such as 10 %, was excluded from concrete experiments due to significant reductions in fluidity, it was retained in cement paste studies to investigate material behavior under extreme conditions. Table 5 lists the cement paste mixture proportions, where 20 cement paste samples were made in total. The mixing procedure of the cement paste adhered to the GB/T 1346–2011 specification [33]. A cement paste mixer was employed for sample preparation, operating at a low speed of 140 r/min for 120 seconds, followed by a high-speed mixing phase at 285 r/min for an additional 120 seconds, with a 15-second pause in between. All cement paste samples were prepared and tested under controlled laboratory conditions, with a temperature of 20 ± 3 °C and a relative humidity of 90 %.

During the second stage of the study, given that the sea sand used was extra-fine with a fineness modulus of 1.23, using the same mix ratio as ordinary river sand would inevitably affect the workability of the SSM. Therefore, the amount of sea sand was decreased and the w/c was raised in order to increase the workability of the SSM in this test. The identical mix ratios used to make the SSM were also used to make the regular sand mortar. The w/c were established at 0.45, 0.5, and 0.55, respectively, and a cement-to-sand ratio of 1:1.5, according to preliminary findings. The percentage of WMP added to the cement dose ranged from 0 % to 10 %. Table 6 details the precise ratios of each mortar sample.

During the experimental program's third stage, investigations were performed to evaluate the influence of hydration parameters and supplementary cementitious material incorporation on the rheological properties and long-term performance of self-consolidating concrete. The experimental matrix was designed with w/c of 0.4, 0.5, and 0.55, while incorporating WMP at varying replacement levels of 0 %, 3 %, and 5 % by mass. By consulting the aggregate ratios found in relevant literature [34], the specific mix ratios for each sample were fine-tuned through trial adjustments. The mix proportion scheme is outlined in Table 7. For mixing the concrete, a biaxial concrete mixer was employed, and test samples were prepared in accordance with Chinese standard "Standard for Test Methods of

Table 1
Main parameters and indexes of cement.

Density(g/cm^3)	Standard consistency(%)	Specific surface area(m^2/kg)	Initial setting time(min)	Final setting time(min)
3.07	27	372	211	264

Table 2
Main chemical compositions of OPC and WMP.

Content	Mass Percentage						
	Al_2O_3	SiO_2	TiO_2	Fe_2O_3	MgO	CaO	Other
OPC	6.35	17.88	0.40	3.72	0.61	66.65	4.39
WMP	72.13	16.32	5.20	1.98	1.53	1.05	1.79

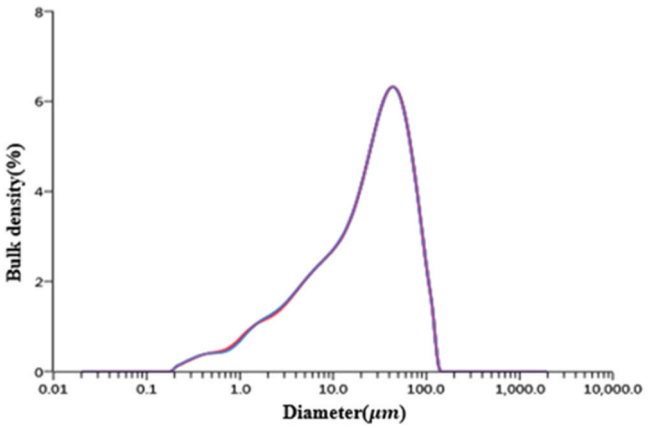

Fig. 1. Particle size distribution of WMP.

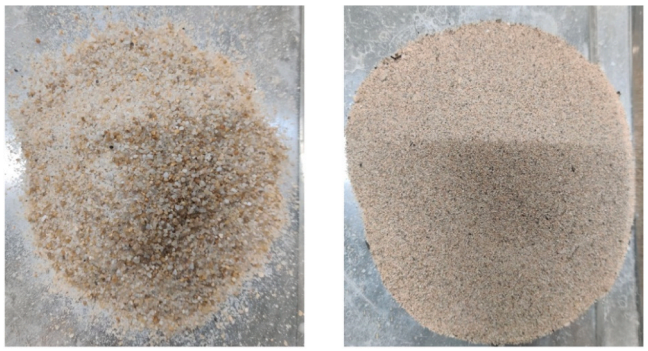

(a) Standard sand (b) Sea sand

Fig. 2. Pictures of different sand samples.

Table 3
Main properties of test sand.

Sand sample	Apparent density(kg/m^3)	Bulk density(kg/m3)	Sediment percentage (%)	Chloride ion content (%)	Fineness modulus	Fineness modulus classification
Standard sand	2650	1570	0.05	0	2.93	Medium sand
Sea sand	2565	1413	0.24	0.3	1.23	Extra fine sand

Table 4
Grading proportion of coarse aggregate.

Particle size range (mm)	5–10	10–15	15–20	20–25
Gradation proportion (%)	30	25	15	30

Table 5
Cement paste mixture proportion.

Sample code	Mixing water	w/c ratio	WMP content (wt%)
F3–0	Freshwater	0.3	0
S3–0	Seawater	0.3	0
S3–3	Seawater	0.3	3
S3–5	Seawater	0.3	5
S3–10	Seawater	0.3	10
F4–0	Freshwater	0.4	0
S4–0	Seawater	0.4	0
S4–3	Seawater	0.4	3
S4–5	Seawater	0.4	5
S4–10	Seawater	0.4	10
F5–0	Freshwater	0.5	0
S5–0	Seawater	0.5	0
S5–3	Seawater	0.5	3
S5–5	Seawater	0.5	5
S5–10	Seawater	0.5	10
F6–0	Freshwater	0.6	0
S6–0	Seawater	0.6	0
S6–3	Seawater	0.6	3
S6–5	Seawater	0.6	5
S6–10	Seawater	0.6	10

Table 6
Cement mortar mix proportion scheme.

Sample number	Seawater(g)	Cement(g)	Standard sand(g)	Sea- sand(g)	WMP(g)	w/c ratio	WMP content(%)
TS45–0	450	1000	1500	0	0	0.45	0
TS45–3	450	1000	1500	0	30	0.45	3
TS45–5	450	1000	1500	0	50	0.45	5
TS45–10	450	1000	1500	0	100	0.45	10
TS50–0	500	1000	1500	0	0	0.5	0
TS50–3	500	1000	1500	0	30	0.5	3
TS50–5	500	1000	1500	0	50	0.5	5
TS50–10	500	1000	1500	0	100	0.5	10
TS55–0	550	1000	1500	0	0	0.55	0
TS55–3	550	1000	1500	0	30	0.55	3
TS55–5	550	1000	1500	0	50	0.55	5
TS55–10	550	1000	1500	0	100	0.55	10
SS45–0	450	1000	0	1500	0	0.45	0
SS45–3	450	1000	0	1500	30	0.45	3
SS45–5	450	1000	0	1500	50	0.45	5
SS45–10	450	1000	0	1500	100	0.45	10
SS50–0	500	1000	0	1500	0	0.5	0
SS50–3	500	1000	0	1500	30	0.5	3
SS50–5	500	1000	0	1500	50	0.5	5
SS50–10	500	1000	0	1500	100	0.5	10
SS55–0	550	1000	0	1500	0	0.55	0
SS55–3	550	1000	0	1500	30	0.55	3
SS55–5	550	1000	0	1500	50	0.55	5
SS55–10	550	1000	0	1500	100	0.55	10

Table 7
Mix proportion of SSC.

Sample number	w/c ratio	Sand rate (%)	Seawater (kg)	Cement (kg)	Sea sand (kg)	Gravel (kg)	WMP (kg)	Water reducing agent (kg)
A−1	0.55	35	253	460	740	1380	0	3.2
A−2	0.55	35	253	460	740	1380	13.8	3.2
A−3	0.55	35	253	460	740	1380	23	3.2
B−1	0.5	33	260	520	670	1367	0	5.2
B−2	0.5	33	260	520	670	1367	15.6	5.2
B−3	0.5	33	260	520	670	1367	26	5.2
C−1	0.4	31	242	604	610	1359	0	7.8
C−2	0.4	31	242	604	610	1359	18.1	7.8
C−3	0.4	31	242	604	610	1359	30.2	7.8

Concrete Physical and Mechanical Properties" GB/T 50081–2019 [34].

2.3. Experimental methods

2.3.1. Yield stress and plastic viscosity

The prepared cement paste was evaluated using an RVDV-1T digital rotational viscometer. The speed of the instrument was gradually raised from 0 to 100 rpm in 10 rpm increments, and then similarly decreased back to 0, with each speed held for approximately 10 seconds. The viscometer recorded the viscosity, shear rate, and the cement paste's shear stress. Rheological characteristics, such as plastic viscosity and yield stress, were determined through computational analysis of flow behavior using the Bingham constitutive model, which was employed to characterize the relationship between shear stress and deformation rate:

$$\tau = \tau_0 + \eta\dot{\gamma} \tag{1}$$

where τ is the shear stress, in Pa; τ_0 is the yield stress, in Pa; η is the plastic viscosity, in $Pa \cdot s$; γ is the shear rate, in s^{-1}. Ultimately, the regression analysis was used to generate the fitting curve, and the corresponding parameters τ_0 and η were identified.

2.3.2. Fluidity

The fluidity of the mortar was measured using the NLD-3 cement mortar fluidity tester in accordance with "Test Method for Fluidity of Cement Mortar" GB/T 2419–2005 [35]. After mixing, the cement mortar was poured into a truncated cone circular mold, which was positioned at the center of the tap table, and the top of the mold was leveled off. The mold was then lifted vertically, and the flowmeter was activated to perform 25 drops. The diameters of the spread mortar along two perpendicular directions were measured using a ruler accurate to 1 mm. The arithmetic average of these two diameters was calculated to determine the fluidity of the cement mortar.

2.3.3. Segregation resistance

The mortar sample's segregation resistance was assessed using a modified sieve segregation resistance test for self-compacting concrete, as described in the "The European Guidelines for Self-Compacting Concrete" [36]. In the modified sieve segregation resistance test, a smaller 1.18 mm sieve was used instead of the 5.0 mm sieve [37,38]. To conduct the test, approximately 0.2 L of mortar sample was taken and weighed (accurate to 0.1 g), and it was allowed to stand without disturbance for 15 minutes. The sample was then poured from a height of 300 mm onto a sieve with a 1.18 mm aperture. Following two minutes of rest, in order to calculate the sieve segregation index (SSI) for the mortar sample under test, the weight of the mortar that flowed through the sieve and was gathered by the base receiver was noted. The following formula ought to be applied when calculating SSI:

$$SSI = \frac{m_2}{m_1} \times 100\% \tag{2}$$

Where m_1 is the total weight of the mortar used in the test, in g; m_2 is the total weight of the mortar that passed through the sieve, in g. Based on Eq. (2), SSI is considered an inverse measure of segregation resistance.

2.3.4. Compressive strength

The mechanical performance evaluation of the cementitious composite was conducted through standardized compression testing utilizing cubic samples measuring 10 cm in each orthogonal dimension, grouped in sets of three. The test procedure followed Chinese standard " Standard for Test Methods of Concrete Physical and Mechanical Properties" GB/T 50081–2019 [34]. The molds were taken out after a day, and the samples were labeled and kept for seven days at 20 ± 2℃ with 95 % relative humidity in a standard curing room. Upon approaching the specified curing age, the concrete samples were tested using the SUNS WAW-1000 with a loading rate of 0.5 MPa/s. The average compressive strength values from the three samples in each group were recorded.

2.3.5. Sulfate resistance of concrete

The sulfate resistance of concrete under drying and wetting cycle conditions was measured using the CABR-LSB fully automatic concrete sulfate resistance testing device, according to "Standard for Test Methods of Long-term Performance and Durability of Ordinary Concrete" GB/T 50082–2019 [39]. A 5 % Na_2SO_4 solution was prepared as the soaking solution. Cubic specimens of cementitious composites with standardized dimensions of 10 centimeters in each orthogonal direction, were organized into five groups, with three blocks per group. One group was designated for measuring the 28-day compressive strength, while two groups were set for compressive strength testing after 30 and 60 dry-wet cycles under Na_2SO_4 solution, respectively. The remaining two groups served as the control groups for compressive strength after the same 30 and 60 dry-wet cycles under distilled water, respectively.

Two days prior to the concrete test blocks reaching 28 days of curing, those designated for the dry-wet cycle group were dried at 80 ± 5°C for 48 hours, then allowed to cool to room temperature. Following this, the blocks underwent the following cycle after being put in a test chamber: For fifteen hours, the blocks were soaked while the temperature was kept at 25 ± 2°C. This was followed by liquid pumping and air drying of the test block for 45 minutes. The temperature was then raised over 30 minutes and maintained at 80 ± 5°C for 5.5 hours. Finally, the blocks were cooled to 25°C over 2 hours, completing a 24-hour dry-wet cycle. This cycle was repeated for a total of 60 cycles. Throughout the testing period, the pH of the soaking solution was measured every 15 cycles to ensure it remained between 6 and 8.

After the concrete test blocks reached the specified curing and testing age, their compressive strength was assessed using the SUNS

WAW-1000 universal testing machine. The durability performance indicator for cementitious materials was quantitatively evaluated through computational analysis employing a standardized mathematical expression to determine the strength preservation ratio under corrosive conditions:

$$K_f = \frac{f_{cn}}{f_{c0}} \times 100\% \tag{3}$$

where K_f is the concrete compressive strength's corrosion resistance coefficient, given as a percentage; f_{cn} is the concrete specimen's compressive strength following n dry-wet cycles and sulfate attack, measured in MPa; and f_{c0}, which is also expressed in MPa, is the concrete test block's compressive strength from the standard curing group at the same age as the block that was attacked by sulfate. The arithmetic average of three test blocks yielded the final compressive strength result, which was accurate to 0.1 MPa.

2.3.6. Chloride ion electric flux test

The measurement of chloride ion migration characteristics in cementitious specimens was performed using the CABR-RCMP6 electrochemical testing system, which simultaneously determines both diffusion coefficients and electrical flux parameters through advanced electrochemical impedance spectroscopy. These blocks were made with cylindrical molds that measured 100 mm in diameter and 100 mm in height. A segment with a height of 50 ± 2 mm was then cut from the cylinder to serve as the test block. Two curing ages, 28 days and 60 days, were designated. Upon reaching the specified curing age, the cylindrical test block was removed from the curing room, its sides coated with epoxy resin glue, and then vacuum-saturated using the CABR-BSY concrete vacuum water saturation instrument. The test block was installed in the test tank to ensure a proper seal. The experimental setup involved the establishment of concentration gradients through the strategic placement of electrolyte solutions, with NaOH solution (0.3 M) and NaCl solution (3.0 % w/w) being added to the testing apparatus's opposing compartments. The NaOH side was attached to the power supply's positive pole, while the side with the NaCl solution was connected to its negative pole. After starting the device, the electrodes on either side of the concrete test block received a steady 60 V DC voltage for six hours. The instrument automatically recorded the current value and calculated the electric flux that passed through the concrete test block over this period. The final result was determined by taking the arithmetic average of the electric flux from three test blocks in each group, accurate to 0.01 C.

2.3.7. Rapid iodide migration

The Rapid Chloride Migration (RCM) test is extensively employed to assess the chloride penetration resistance of concrete, offering greater accuracy than the electric flux method [40]. However, challenges were encountered during the application of the RCM method in this study, particularly in delineating the color-developing boundary of AgCl precipitation (white). The pervasive presence of chloride in the sea sand and seawater led to the entire sample section turning white, as illustrated in Fig. 3a. As a result, this interference compromised the effectiveness of the RCM method in precisely evaluating chloride penetration.

Due to the low iodine ion content in concrete components, Liu et al. [38] proposed using iodine ions as a substitute for chloride ions to evaluate the ionic permeability resistance of concrete. The RCMP6-CAB migration analyzer, functioning on non-steady-state electrochemical principles, was utilized to quantify both ionic penetration coefficients and coulombic flux values in hydrated cement systems, with test block preparation and curing procedures consistent with Section 2.3.6. Prior to testing, the concrete block should be vacuum saturated and then placed into a rubber sleeve to ensure a snug fit. In the cathode test tank, a 0.2 mol/L KOH solution containing 12 % NaI was added, while the anode tank was filled with a 0.2 mol/L KOH solution. Both tanks were covered with black plastic bags to shield them from light. A 30 V DC voltage was applied, the initial current was recorded, and the actual test voltage and time were automatically adjusted. Following the test, the specimen was moved to a testing apparatus, where it was divided into two semi-cylindrical sections along the axis. A 50 % mass concentration acetic acid solution was sprayed on the profile for acidification and left for 1 minute. Subsequently, a 3 % mass concentration potassium iodate solution was sprayed on the profile, immediately followed by a 5 % mass concentration soluble starch solution. The section then exhibited a blue-purple precipitate. The profile of the test block was split into ten equal sections along its diameter, the color boundary was marked, and the distance—to within 0.1 mm—between the boundary and the test block's bottom was measured, as depicted in Fig. 3b.

Excluding data where the percentage difference exceeds 15 %, the average color rendering depth of the remaining measurement points is taken as the final result. This value is then used in the following formula to calculate the iodide diffusion coefficient:

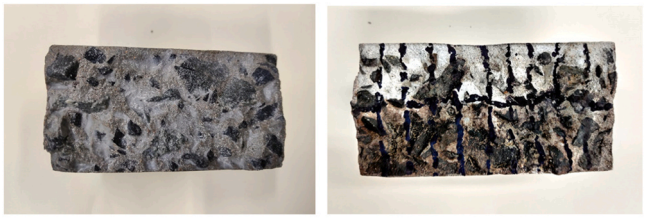

a) RCM test block. b) RIM test block

Fig. 3. test block for RCM and RIM.

$$D = 2.872 \times 10^{-6} \frac{Th\left(x_d - \alpha\sqrt{x_d}\right)}{t} \tag{4}$$

where D represents the iodide diffusion coefficient, in m^2/s; T is the average temperature of the anode solution, in K; h is the height of concrete test block, in m; x_d represents the depth of color rendering for the specimen under examination, in m; t is the power on duration, in s; α is the auxiliary variable, $\alpha = 3.338 \times 10^{-3}\sqrt{Th}$.

2.3.8. Microstructure characterization

The hydration products of F4–0, S4–0, S4–3 and S4–5 samples at the age of 3days, 7days and 28days were examined by scanning electron microscope (SEM) to observe the microstructure morphology, and they were also investigated by Scanning Electron Microscopy (XRD) and Energy-Dispersive (EDS) X-Ray Microanalysis, thermal gravimetric analysis (TGA) and Fourier transform infrared spectrometer (FTIR) to analyze the compositions. For the TGA, During the heating process of cement paste sample, three major weight losses occur. The first occurs between 50℃ to 200℃, where the mass loss is mainly due to the evaporation of free water adsorbed in the cement pores and the depletion of bound water from C-S-H gel and ettringite (AFt). The second mass loss takes place between 380℃ to 460℃, within this temperature range, the dehydration and decomposition of calcium hydroxide (CH) to form CaO causes significant weight loss. When the temperature rises to the range of 650℃ to700℃, $CaCO_3$, which is formed by the carbonation of CH, decomposes into CaO upon heating, releasing CO_2 and causing a decrease in the TG curve. Since part of the CH is carbonated to form CaCO3, it is assumed that the mass fraction of CH undergoing dehydration in the range of 380℃ to 460℃ is A, and the mass fraction of CaCO3 decomposing in the range of 650℃ to 700℃ is B. Thus, the CH content of the former (W_1) can be calculated:

$$W_1 = A \times \frac{74}{18} \tag{5}$$

The CH content of the latter (W_2) is:

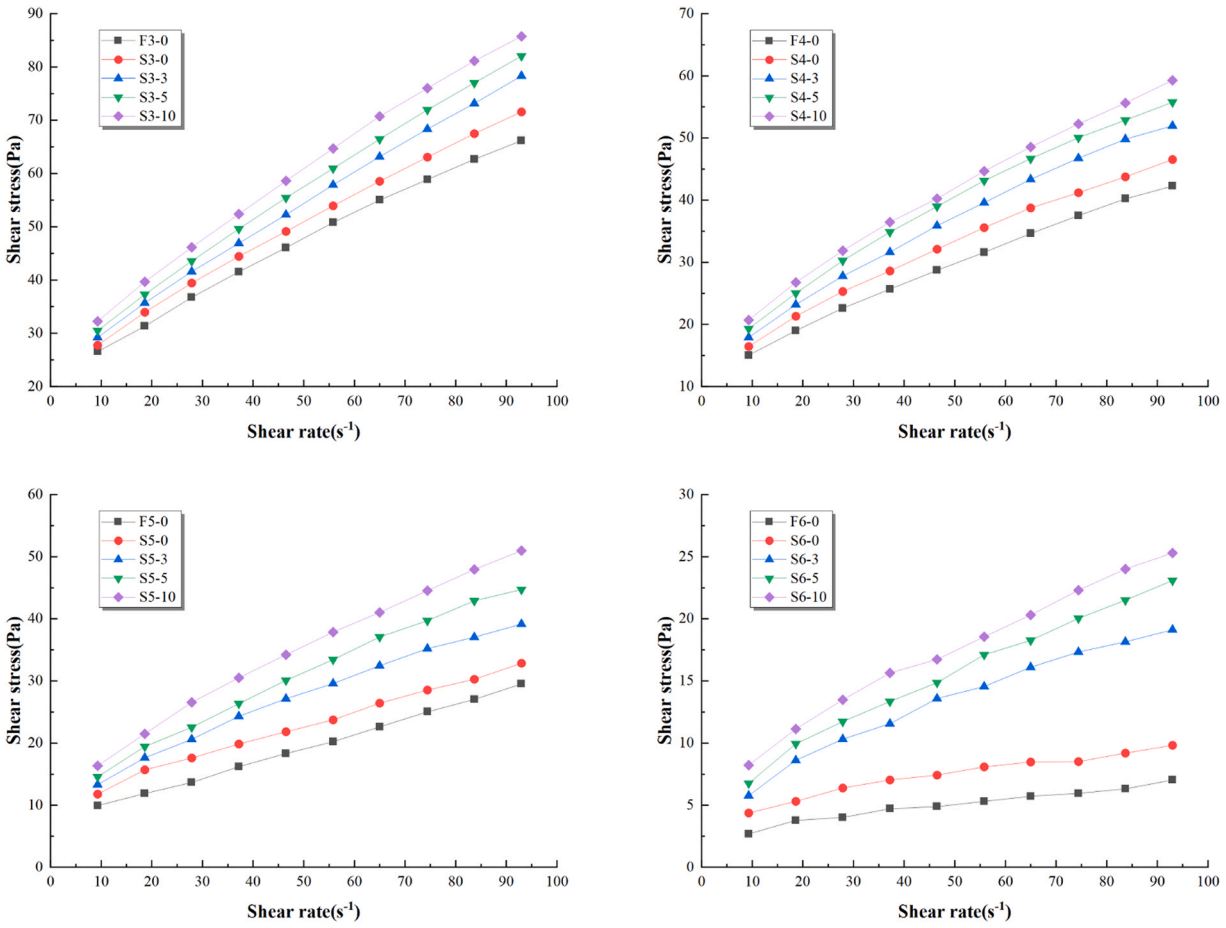

Fig. 4. Shear stress and shear rate relationship of cement paste under different w/c ratio.

$$W_2 = B \times \frac{74}{44} \tag{6}$$

Therefore, the total mass fraction of CH in the sample (W) is:

$$W = W_1 + W_2 \tag{7}$$

3. Results and discussion

3.1. Rheological properties

3.1.1. Shear stress and shear rate

The shear stress-shear rate values for cementitious composites engineered with systematically varied w/c (0.3, 0.4, 0.5, 0.6), mixed under different conditions of mixing water and WMP content at normal temperature, were recorded, as displayed in Fig. 4. Under identical w/c and shear rates, compared to cement paste mixed with freshwater, the shear stress of SCP was higher. Furthermore, as the WMP content rose in the SCP, the shear stress increased steadily at the same shear rate. Because seawater is rich in sulfate and sulfite ions, these ions rapidly react with the cement hydration products within minutes of mixing, forming AFt [41]. This reaction increases the internal AFt content in the SCP compared to paste mixed with freshwater, thus resulting in greater slurry consistency. The shear stress in cement paste reflects the impeding effect between particles. The addition of WMP enhances the friction and collisions among particles, increasing the loss of van der Waals forces and kinetic energy, which in turn raises the shear stress of the paste.

As the w/c rises at the same shear rate, the cement paste's shear stress steadily falls while the amount of WMP stays constant. This reduction in shear stress is due to the decreased content of cementitious materials and particles, and the increased content of free water, which results in greater internal particle spacing. Consequently, the kinetic energy loss from friction and collisions among particles in the paste is reduced, leading to lower shear stress. Initially, at low shear rates and over short periods, the difference in shear stress among cement pastes with varying w/c and WMP content is not pronounced. However, as the shear rate increases, a more noticeable difference emerges. This phenomenon occurs because, at low shear rates, particle agglomeration and sedimentation may take place at the start of agitation, leading to minimal differences in shear stress. After the rotor has been in operation for some time, these agglomerated and settled particles are stirred and dispersed again, resulting in significant differences under higher shear rates.

The observed linear trend in the flow characteristics of the cementitious mixture suggests that the fluid dynamics of the cement composite incorporating WMP additives conform to the principles of the Bingham plastic model. The yield stress and plastic viscosity are determined using the formulations derived from the fitted Bingham model, as detailed in Table 8.

3.1.2. Yield stress and plastic viscosity

Yield stress is the maximum resistance that must be overcome to initiate the flow of a fluid, primarily arising from the attraction and friction between particles within the cement paste. It serves as a measure of the bonding strength between particles in the paste and reflects the difficulty of initiating flow from a macroscopic perspective. Plastic viscosity relates to particle obstruction within the cement paste. Its magnitude depends on the compactness of the flocculation structure. This parameter indicates the difficulty encountered during the flow process, also from a macroscopic perspective.

Fig. 5 illustrates the yield stress and plastic viscosity of cement pastes made with freshwater and seawater across various w/c. At identical w/c, compared to the freshwater cement paste, the SCP had a higher yield stress and plastic viscosity. In particular, for w/c of

Table 8
Bingham fitting parameters of cement paste containing WMP.

Sample number	R^2	Yield stress τ_0(Pa)	Plastic viscosity η(Pa·s)
F3–0	0.9961	23.16	0.477
S3–0	0.9973	24.44	0.518
S3–3	0.9988	24.90	0.582
S3–5	0.9981	26.15	0.613
S3–10	0.9965	27.99	0.641
F4–0	0.9955	13.12	0.325
S4–0	0.9912	14.91	0.353
S4–3	0.9913	15.90	0.408
S4–5	0.9871	17.63	0.431
S4–10	0.9932	18.56	0.451
F5–0	0.9989	7.44	0.235
S5–0	0.9952	10.59	0.240
S5–3	0.9989	12.04	0.305
S5–5	0.9933	12.54	0.363
S5–10	0.9927	14.41	0.406
F6–0	0.9719	2.71	0.046
S6–0	0.9612	4.40	0.060
S6–3	0.9786	5.63	0.154
S6–5	0.9916	6.12	0.187
S6–10	0.9914	7.45	0.198

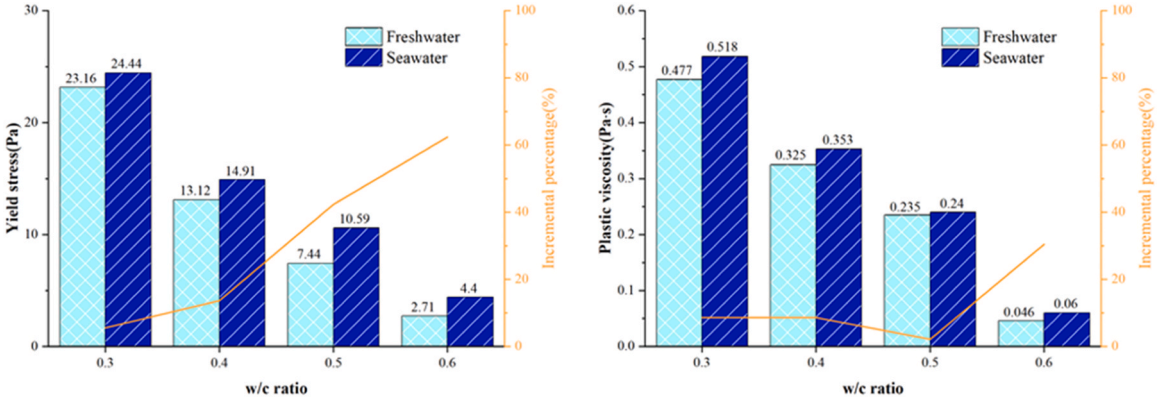

Fig. 5. Yield stress and plastic viscosity versus different mixing water under different w/c ratios.

0.3, 0.4, 0.5, and 0.6, the yield stress of the SCP rose by 6 %, 14 %, 42 %, and 62 %, respectively, but the plastic viscosity increased by 8 %, 9 %, 2 %, and 30 %, respectively. Dissolved salts in seawater increase interparticle attraction and friction, significantly raising the yield stress. However, their limited effect on particle dispersion and flow structure results in relatively minor changes in plastic viscosity, making the influence of seawater more pronounced on yield stress than on plastic viscosity. Additionally, the impact of seawater on the rheological characteristics of the cement pastes increased as the w/c rose.

Fig. 6 displays the yield stress and plastic viscosity for various WMP contents and w/c. As the WMP content rose, so did the cement paste's yield stress and plastic viscosity. For instance, at a w/c of 0.3, the yield stress for SCP mixed with 3 %, 5 %, and 10 % WMP increased by 2 %, 7 %, and 15 % respectively, while the plastic viscosity increased by 12 %, 18 %, and 24 % respectively, compared to the cement paste without WMP. The addition of WMP introduces more solid particles into the cement paste system, effectively reducing the w/c and significantly enhancing both yield stress and plastic viscosity. The specific surface area within the cement paste system is increased by the addition of WMP, resulting in higher water demand and a reduction in the free water content, which typically acts as a lubricant between solid particles. Consequently, the thickness of the water film coating the particle surfaces decreases, greatly enhancing the likelihood of particle collisions and the resistance that must be overcome during internal sliding, thereby elevating the yield stress. Furthermore, according to the crystal growth theory, the inclusion of WMP provides additional nucleation sites for the growth of C-S-H gel, accelerating the formation of hydration products. The reinforcement of the internal agglomeration network within the cementitious matrix intensifies the intermolecular frictional resistance among particulate constituents, impeding their movement and thus increasing the plastic viscosity. Ultimately, the incorporation of WMP negatively impacts the rheological properties of the cement paste.

3.2. Fluidity

Fig. 7 displays the fluidity of standard sand mortar and SSM, varying across different WMP contents and w/c. Within the same WMP content levels, the fluidity of both standard sand and SSM improved as the w/c increased. This trend indicates a positive correlation between the fluidity of mortar, irrespective of the sand type used, and its w/c. The rise in the w/c enhances the free water content

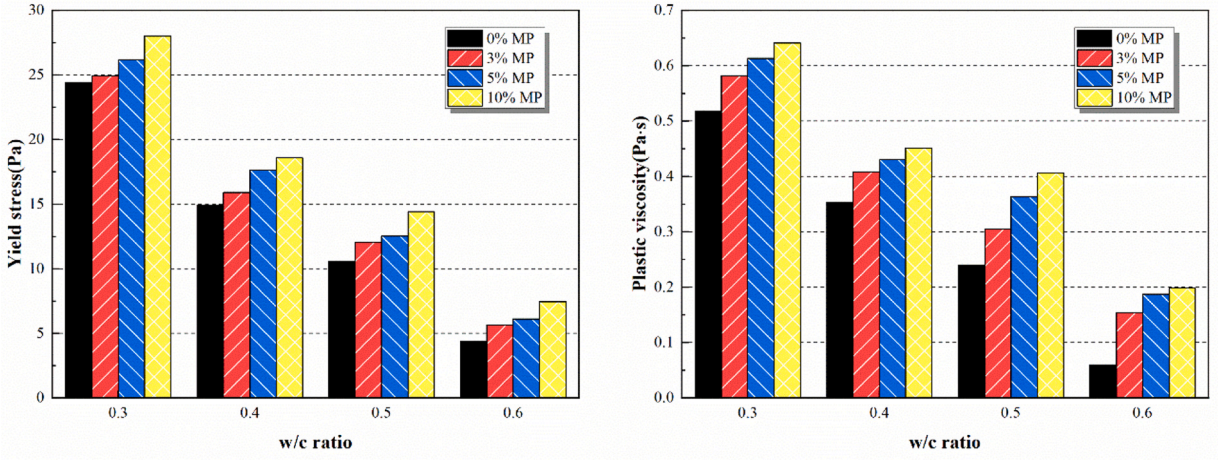

Fig. 6. Yield stress and plastic viscosity versus content of WMP under different w/c ratios (SCP).

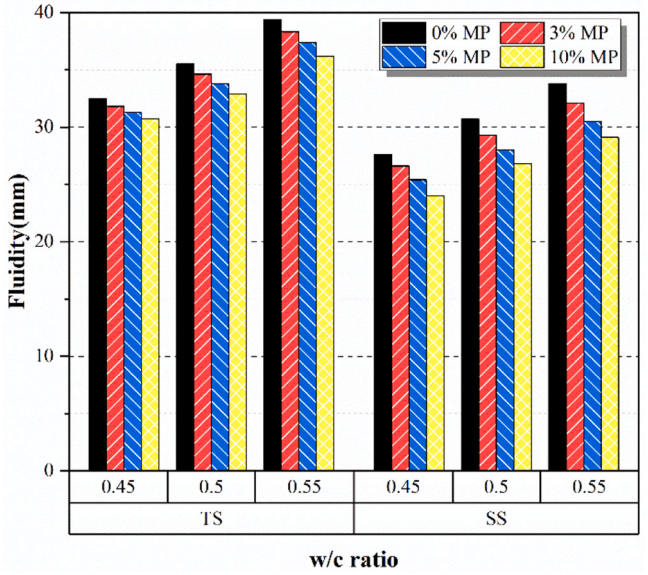

Fig. 7. Fluidity of standard sand (TS) and sea sand (SS) mortar with different content of WMP under different w/c ratios.

within the mortar, serving a lubricating function. It also increases the spacing between the cementitious materials and sand particles, which diminishes the resistance from collision friction, thereby boosting the fluidity of the mortar.

Maintaining consistent w/c, compared to regular sand mortar with the same WMP content, SSM had less fluidity. This indicates that achieving comparable fluidity with sea sand requires a higher water mix compared to standard sand, aligning with the findings of Limeir et al. [42]. This difference is primarily due to sea sand having a smaller fineness modulus than standard sand, which increases the specific surface area of the particles in the mortar, thereby raising the water demand. Additionally, the smaller particles of sea sand heighten the likelihood of collisions between particles in the mortar, further increasing the flow resistance.

While the influence of WMP on the fluidity of mortar is not as pronounced as that of the w/c and sand type, it still exhibits a consistent pattern. For mortar using the same sand, fluidity decreased with increasing WMP content at a constant w/c, indicating that WMP addition negatively affects mortar fluidity. Introducing WMP raises the yield stress and plastic viscosity of the cement paste, thereby improving the adhesion and friction among sand particles. This increase in friction raises the resistance to particle sliding, consequently reducing the rheology of the mortar.

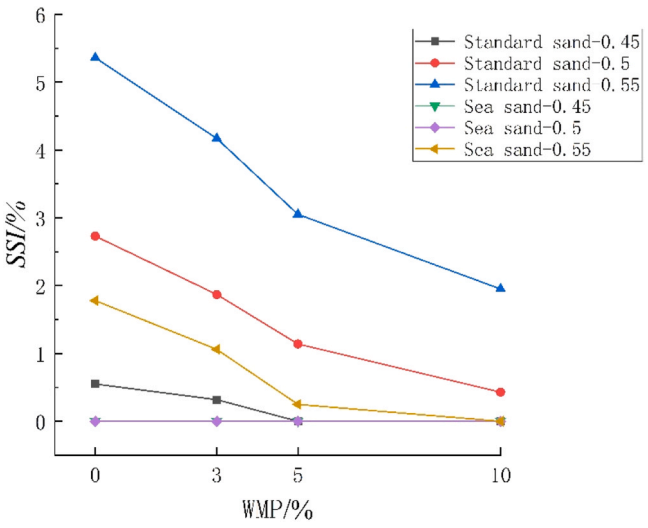

Fig. 8. SSI of mortar with different content of WMP under different w/c ratios.

3.3. Segregation resistance

Fig. 8 displays the *SSI* of with standard sand mortar and SSM. The sieve segregation resistance test indicates that both standard sand mortar and SSM exhibit relatively high segregation resistance. The highest *SSI* observed was for standard sand mortar with a w/c of 0.55, indicating that only 5.36 % of the total mass of the sample passed through the 1.18 mm sieve. For most SSM samples, the *SSI* was 0, indicating that these samples did not pass through the 1.18 mm sieve at all, suggesting minimal segregation and bleeding, which provides valuable guidance for using sea sand as fine aggregate in concrete mixing.

Based on an analysis of different variables, it can be seen that: (1) For the same type of sand and the same amount of WMP, there is a significant difference in the *SSI* between different w/c. The results were mainly analyzed for standard sand mortar because most SSM indices are 0. In the three groups of standard sand mortar without WMP, the *SSI* at w/c of 0.45, 0.5, and 0.55 are 0.55 %, 2.73 %, and 5.36 %, respectively, showing that reducing the w/c is an effective way to improve the segregation resistance of cement mortar. (2) For the same type of sand at the same w/c, the *SSI* decreases with an increase in WMP content, indicating that the addition of WMP also improves mortar segregation resistance, though not as effectively as reducing the w/c. (3) The segregation resistance of SSM is better than that of standard sand mortar, primarily due to the smaller fineness modulus of sea sand, which absorbs a significant amount of free water on the particle surfaces and raises the specific surface area inside the mortar, macroscopically resulting in a thicker mortar with virtually no bleeding.

3.4. Slump and spread

The slump and spread of SSC were inversely proportional to the WMP content, as indicated in Table 9. As the WMP content increased, the fluidity of the concrete deteriorated. Specifically, the slump of concrete decreased by 7.7 %, 8.6 %, and 7.4 %, respectively, with w/c of 0.55, 0.5, and 0.45 as the WMP content increased from 0 % to 5 %. Similarly, the spread decreased by 5.4 %, 7.3 %, and 6.6 % respectively. The sea sand used in the concrete, having a small fineness modulus and a large specific surface area, required more water than standard sand concrete. Consequently, the increased surface energy of the particles led to a higher water demand. To maintain the concrete's strength and durability while keeping the w/c ratio unchanged, water-reducing agents were added at rates of 0.7 %, 1.0 %, and 1.3 % for w/c of 0.55, 0.5, and 0.4, respectively, to enhance workability. After these adjustments, the slump of the concrete reached over 150 mm, satisfying the fluidity requirements for engineering practice.

3.5. Compressive strength

Fig. 9 displays the 28-day compressive strength of SSC with different w/c and WMP dosages. In general, SSC's compressive strength increased after 28 days, and it increased with higher WMP content. Concrete's compressive strength rose 1.7 % and 3.9 % with the addition of 3 % and 5 % WMP, respectively, at a w/c of 0.4. 3.1 %, 6 %, and 3.3 %, 5.3 % increases were seen for w/c of 0.5 and 0.55, respectively. The effect was more noticeable in concrete with a higher w/c, even though the percentage increase in compressive strength brought on by WMP was largely constant across all w/c. In comparison to concrete with a lower w/c, concrete with a greater ratio has more free water, which results in less compactness. Thus, in such concrete, the filling effect of WMP is more important, leading to a more noticeable increase in compressive strength. The change pattern of the 7-day compressive strength of SSC with varying w/c and WMP dosages is similar to the 28-day, which increases with the increase of WMP content.

3.6. Sulfate resistance of concrete under dry-wet cycle

To assess the sulfate resistance of SSC under 30 dry-wet cycles, the compressive strength of test blocks from the KS30 test group and the general curing control group was measured. Similarly, after 60 dry-wet cycles, the compressive strength of test blocks from the KS60 test group and the general curing control group was measured. The compressive strength values were then substituted into Eq. (3) to calculate the corrosion resistance coefficient of concrete compressive strength, with the results presented in Fig. 10.

Following 30 cycles of dry-wet transitions, the sulfate resistance assessment revealed that the compressive strength of the SSC specimens within both the test and control groups exhibited higher values compared to those of the 28-day samples (see Fig. 9). The compressive strength of each test block increased with higher WMP content, with a more pronounced effect at higher w/c. Following

Table 9
Slump and spread of SSC.

Sample number	Slump(mm)	Spread(mm)
A−1	195	370
A−2	187	363
A−3	180	350
B−1	185	354
B−2	176	341
B−3	169	328
C−1	163	318
C−2	157	310
C−3	151	297

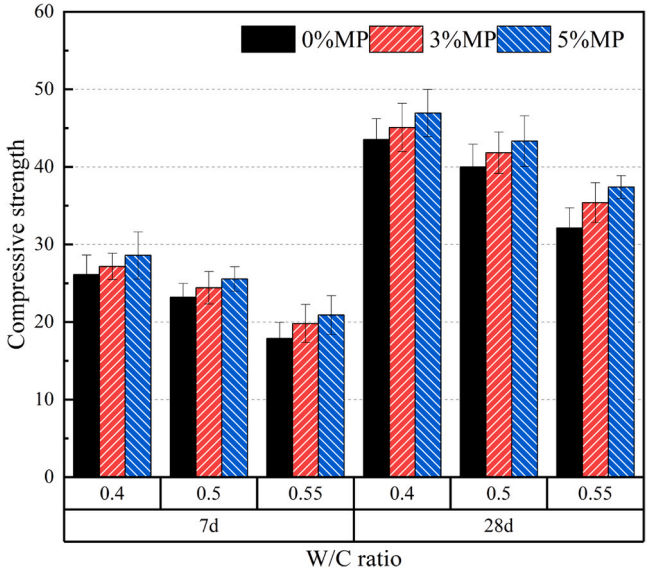

Fig. 9. 7-day and 28-day compressive strength of sea sand seawater concrete.

30 cycles of sulfate erosion, the corrosion resistance coefficient of concrete in the test group for each ratio reached approximately 102 %. This indicates that the concrete's strength continued to increase during the early dry-wet cycles under sulfate exposure.

AFt can form during the early stages of sulfate erosion when high temperatures and humidity levels cause cement to undergo a hydration reaction [43]. The subsequent continuous precipitation of AFt crystals within the internal pores of SSC, in conjunction with the filling effect of WMP, causes the interface transition zone between the cement paste and the aggregate to become compacted and densified. This procedure improves the internal structure's compactness by decreasing the size of the internal pores and microcracks. Consequently, the concrete's compressive strength rises faster than it would if it were cured under normal circumstances.

The C-S-H gel is gradually broken down by sulfate intrusion [44], but the rate at which AFt forms during the early erosion process is greater than the rate at which the C-S-H gel breaks down. As a result, the concrete's internal structure becomes more stable and compact. Consequently, the compressive strength of SSC was marginally enhanced by early sulfate erosion.

The corrosion resistance coefficient of concrete in each mix proportion had fallen below 100 % after 60 dry-wet cycles, according to the sulfate resistance of SSC, indicating a decrease in compressive strength brought on by sulfate erosion. For w/c of 0.55, 0.5, and 0.4 water to cement, the average corrosion resistance coefficients were 95.3 %, 96.39 %, and 97.6 %, respectively. Sulfate corrosion was more likely to occur in concrete with a higher w/c, resulting in a greater reduction in compressive strength compared to concrete with a lower w/c.

The decrease was observed due to the higher extent of sulfate penetration as the dry-wet cycles increased, accelerating the decomposition of the C-S-H gel and reducing the stability of the internal concrete structure. The deposition of erosion products in the concrete increased the sulfate concentration in the pores, leading to crystal precipitation. These crystals kept forming and gradually occupied the internal voids within the concrete [45].

At this stage, the internal voids within the concrete started to undergo stress from expansion. When the internal strength of the concrete could no longer withstand this expansion stress, the internal structure was compromised. Pores and cracks formed, and the erosion products started to fill these newly created voids. The combined effects of filling and destruction influenced the internal structure of the concrete, causing a slight decrease in its compressive strength.

3.7. Concrete's chloride ion electric flux

As demonstrated in Fig. 11, the investigation of chloride ion electric flux for SSC at curing ages of 28 days and 60 days under varying ratios yielded notable findings. At 28 days, a substantial decline in electric flux was observed with a decrease in the w/c. For w/c of 0.55, 0.5, and 0.4, the average electric flux values were 3175.51 C, 1915.43 C, and 992.53 C, with decrease percentages of 40 % and 48 %, respectively. When the WMP content increased from 0 % to 5 % in concrete samples with w/c of 0.55, 0.5, and 0.4, the electric flux decreased by 367.19 C, 439.76 C, and 325.63 C, respectively. This finding suggests that, for a given w/c, the electric flux of concrete samples decreases as the WMP content increases, thereby demonstrating that the WMP enhances the chloride ion permeability resistance of concrete.

At the 60 days, the electric flux outcomes followed a similar trajectory to those observed at the 28 days. The decline in the w/c, concomitant with the augmentation in WMP content, resulted in a decline in the electric flux of the concrete. At 60 days, the average electric flux values for concrete samples with w/c of 0.55, 0.5, and 0.4 were 1989.07 C, 1374.28 C, and 877.28 C, with decrease percentages of 31 % and 36 %, respectively. The percentage change in electric flux at 60 days was less than that at 28 days. For

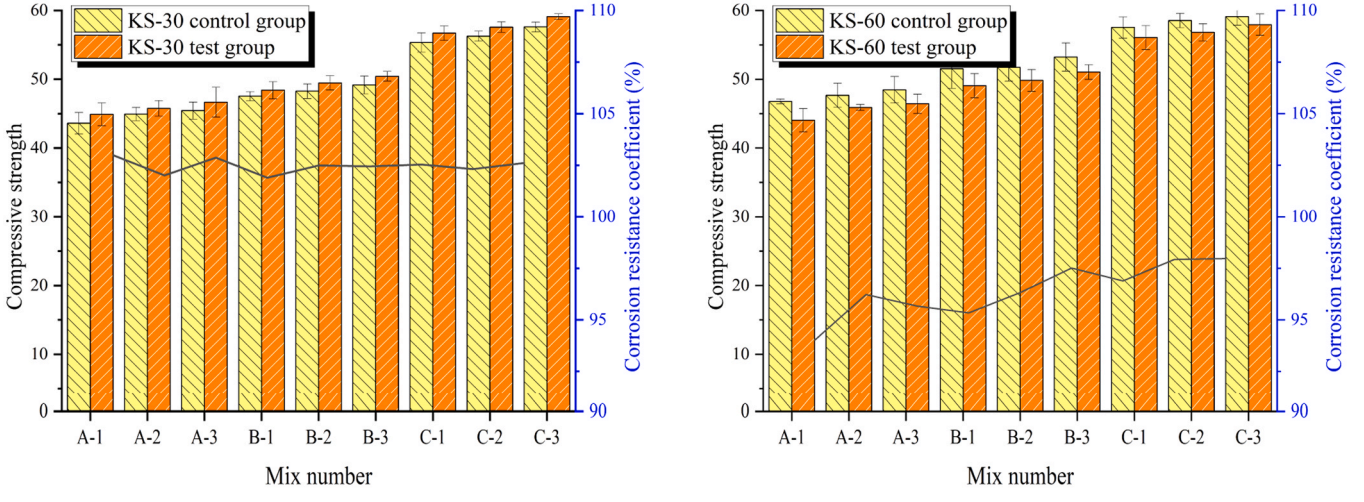

Fig. 10. Corrosion resistance coefficient of concrete compressive strength under different test groups.

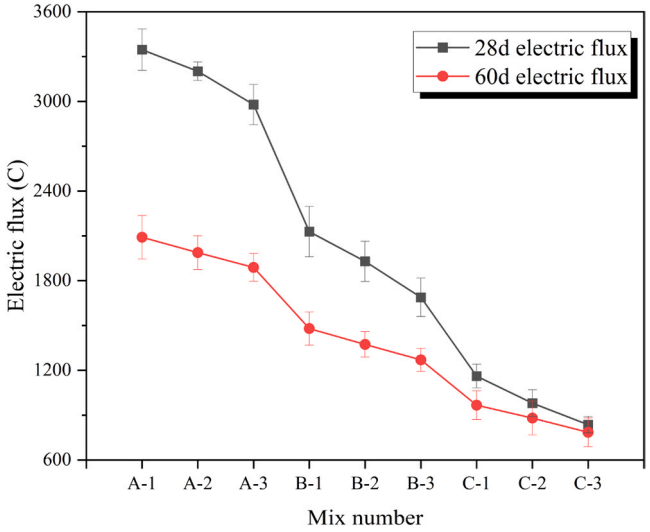

Fig. 11. Chloride ion electric flux of concrete at different ages.

concrete samples with w/c of 0.55, 0.5, and 0.4, the increase in WMP content from 0 % to 5 % resulted in electric flux decreases of 201.55 C, 209.91 C, and 182.04 C, respectively. In comparison with the reduction in electric flux at 28 days, the reduction at 60 days was less pronounced.

3.8. Rapid iodide migration

The iodide penetration depth of SSC at the curing age of 28d and 60d under different proportions was obtained, which was substituted into the formula, and the calculated results of rapid iodide diffusion coefficient were shown in Fig. 12. It was discovered that when the w/c decreased, the RIM diffusion coefficient decreased proportionately. At 28 days, the average RIM diffusion coefficient dropped by 22 % and 36 % for concrete samples with w/c of 0.55, 0.5, and 0.4, respectively. The average RIM diffusion coefficient dropped by 15 % and 35 %, respectively, at 60 days. It was discovered that the decline in the w/c caused the RIM diffusion coefficient to decrease in an age-dependent manner, with longer curing ages resulting in a smaller reduction in concrete samples. Furthermore, an increase in WMP content was observed to result in a decrease in RIM diffusion coefficient, suggesting that WMP exerts an inhibitory effect on the permeability of iodine ions. This finding indicates that WMP can potentially prevent or control the invasion of chemical ions in the environment, thereby enhancing the durability of concrete. To sum up, RIM method had a good evaluation effect on the ion permeability of SSC samples and it was feasible to use iodide ion instead of chloride ion as the permeability ion.

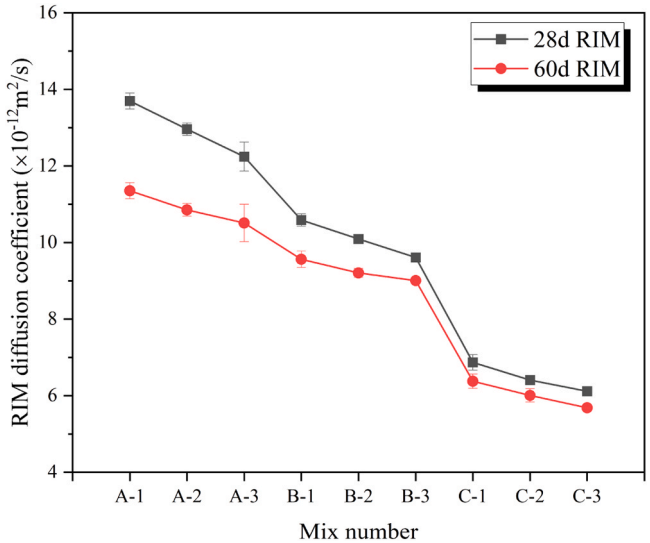

Fig. 12. RIM measurement results of concrete at different ages.

The mechanism of adding WMP on chloride ion permeability resistance of SSC was studied as follows. In the hydration process of ordinary Portland cement, it is generally believed that the C_3A component in cement is mainly combined with the chloride ion. Theoretically, the chloride ions reacted with CH obtained by hydration of C_3S to produce $CaCl_2$, and then $CaCl_2$ reacted with C_3A to obtain Friedel's salt. When the content of C_3A in cement was high, the reaction first produced high chlorine hydrated calcium chloroaluminate ($3CaO{\cdot}Al_2O_3{\cdot}3CaCl_2{\cdot}30\ H_2O$). When the amount of C_3A decreased after a period of reaction, the low chlorine hydrated calcium chloroaluminate ($3CaO{\cdot}Al_2O_3{\cdot}CaCl_2{\cdot}10\ H_2O$) would be generated. The related chemical equation was as follows:

$$2(C_3S) + 6H_20 \Rightarrow C_3S_2H_3 + 3Ca(OH)_2 \tag{8}$$

$$Ca(OH)_2 + 2Cl^- \Leftrightarrow CaCl_2 + 2OH^- \tag{9}$$

$$C_3A + 3CaCl_2 + 30H_2O \Leftrightarrow 3CaO \cdot Al_2O_3 \cdot 3CaCl_2 \cdot 30H_2O \tag{10}$$

$$C_3A + CaCl_2 + 10H_2O \Leftrightarrow 3CaO \cdot Al_2O_3 \cdot CaCl_2 \cdot 10H_2O \tag{11}$$

Since the sea water and sea sand contained chloride ions, Al_2O_3, the main chemical component of WMP, can accelerate the reaction of Friedel' salt, which played a certain role in fixing the chloride ions. Simultaneously, the cement hydration kinetics were significantly enhanced, resulting in accelerated setting characteristics and reduced hardening duration of the cementitious composite. Xu et al. [26]

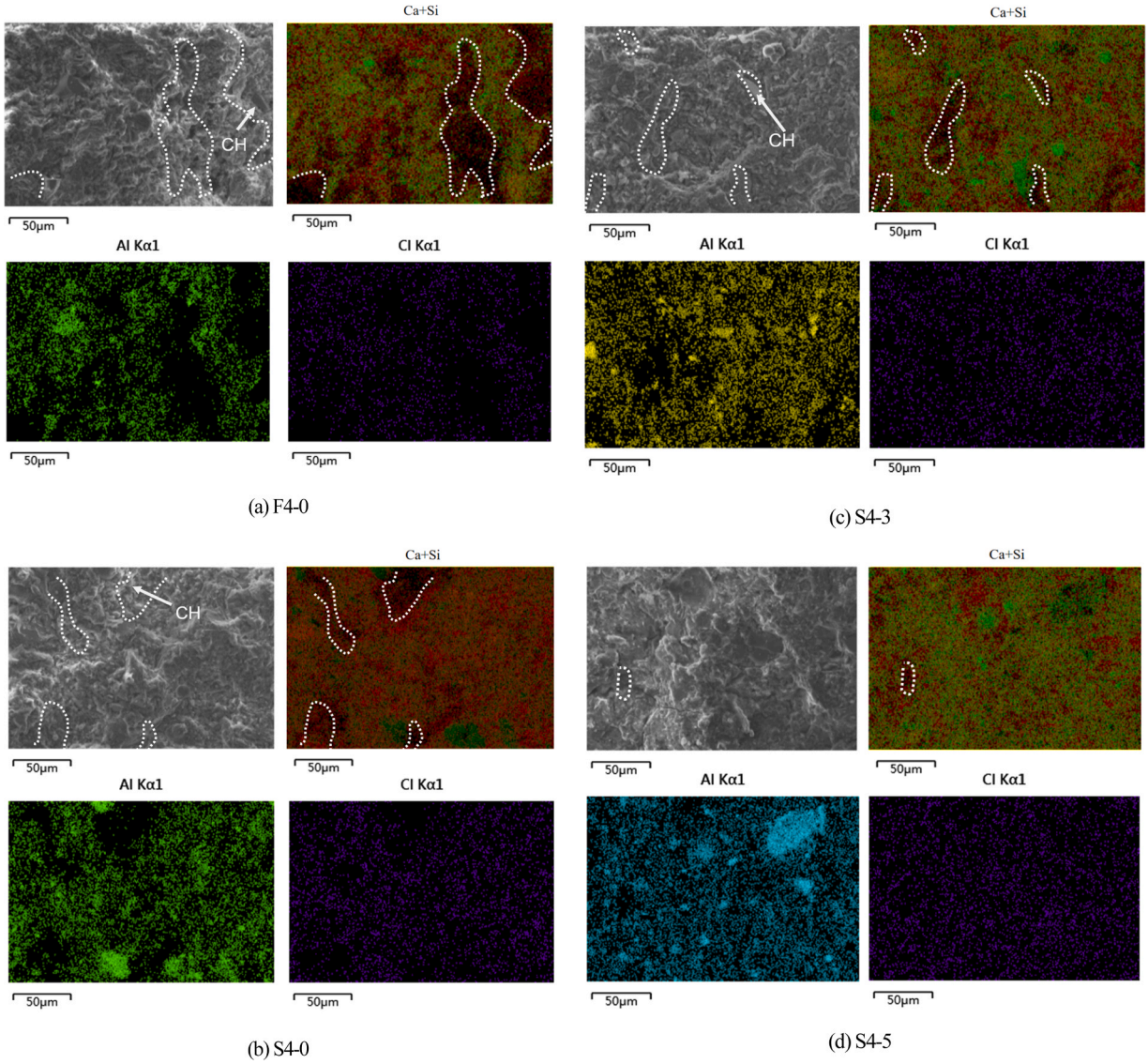

Fig. 13. Microstructure morphology at 3 days.

demonstrated that Al_2O_3 present in WMP significantly improves the chloride ion penetration resistance of concrete through two primary mechanisms: (1) promoting the formation of C-A-S-H gel and (2) providing a physical filling effect, analogous to the behavior observed in volcanic ash materials such as fly ash. Furthermore, WMP's microaggregate filling effect contributes to pore structure refinement. In accordance with Wang et al. [46], the addition of aluminum phase can change the polymerization structure of C-S-H gel. The aluminum atoms replaced part of the silicon atoms of silicon chain in C-S-H gel, so that the silicon chain can be transformed into the aluminum-silicon chain with better polymerization effect, which encouraged the conversion of C-S-H gel into C-A-S-H gel and raised the degree of polymerization of the cementitious composites' microstructural architecture. Combined with the research of Marie et al. [47] the aluminum-silicon chain in C-A-S-H gel had stronger ability to attract cations (Na^+, Ca^{2+}) than the silicon chain in C-S-H gel. The substitution of aluminum atoms increased the electronegativity of unbridged oxygen atoms in C-A-S-H gel, so there were more cations distributed on the surface of C-A-S-H gel to balance the negative charge generated by it. However, as the number of cations on the C-A-S-H gel interface increased, more chloride ions combined with these cations to form ion clusters. These ion clusters reduced the quantity of free chloride ions in concrete, inhibited the infiltration of foreign chloride ions, and had a potent adsorption effect on chloride ions. Furthermore, the pore structure of concrete benefited from the filling and micro-aggregate effects of WMP. Concrete's internal pore structure and mesh frame were reinforced, and its strength characteristics and resistance to the infiltration of external chloride ions were improved as a result of the interpenetration and combination of WMP and cement hydration products, which filled the concrete's tiny pores with insoluble products. Simultaneously, SSC's internal chloride ion had a specific concentration, and because of the influence of the concentration difference between the identical ions, the ion diffusion rate of the external chloride ion was marginally slower than that of ordinary concrete. Thus, in one sense, adding WMP to concrete increases the density of its internal

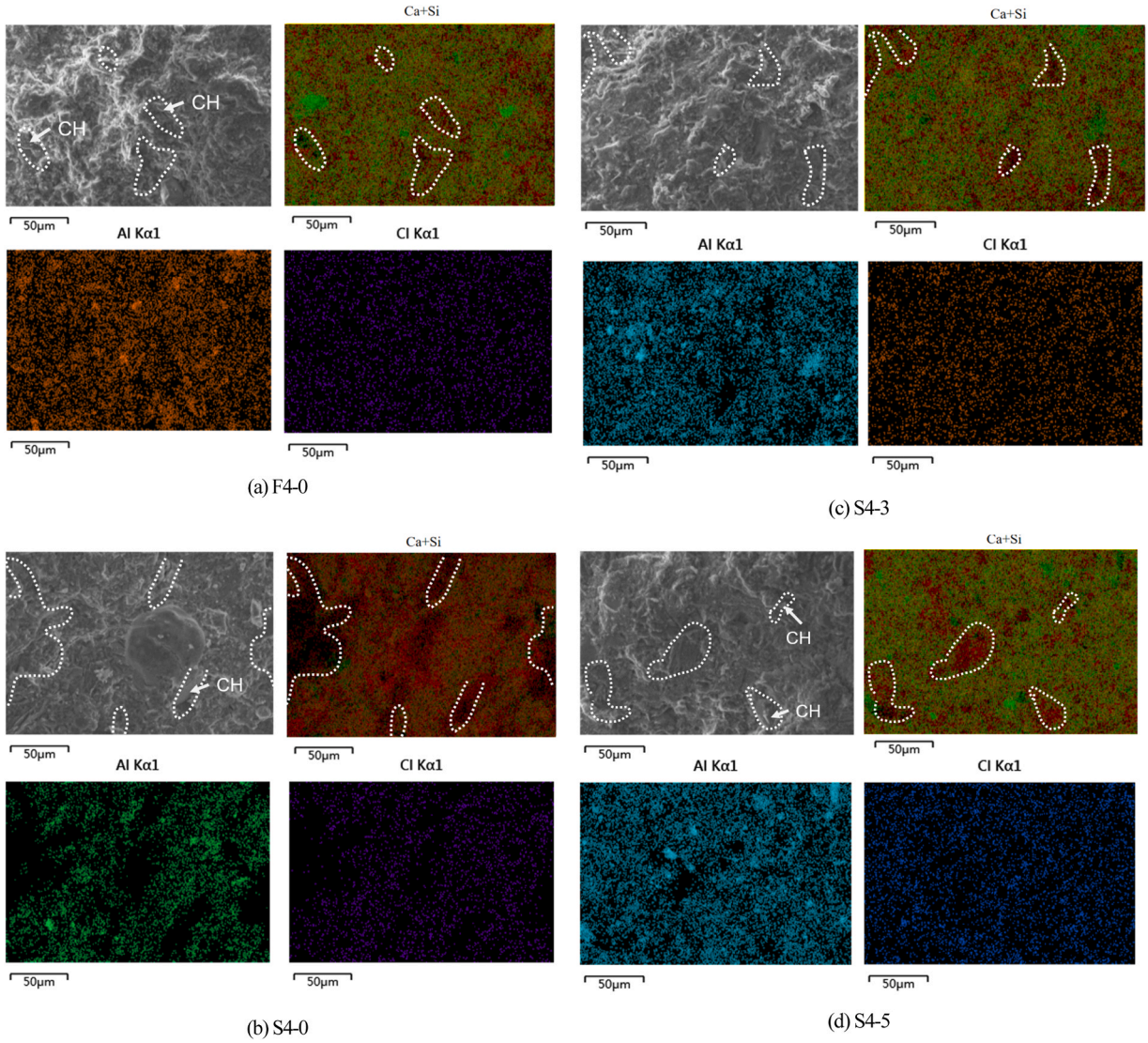

Fig. 14. Microstructure morphology at 7 days.

structure by reducing the formation of micropores and fractures within the material. However, it had a physical adsorption and fixing impact on the chloride ions in SSC, which enhanced SSC's resistance to chloride ion permeability and enhanced concrete's durability.

3.9. Microstructure characterization

3.9.1. SEM and EDS

In this study, SEM was used for microanalysis of the hydration products, while Huang et al. [48] further verified the improvement of microstructure by observing the interfacial behavior of the fibers and seawater sea sand engineered/strain-hardening cementitious composites matrix through SEM.

The co-distribution of Si^{2+} and Ca^{2+} suggests regions predominantly composed of C-S-H or C-A-S-H gel, as shown in the merged elemental maps in Figs. 13 to 15. Areas exhibiting strong Ca^{2+} signals but weak or absent Si^{2+} signals are indicative of CH, as highlighted in the corresponding figures. The simultaneous presence of Al^{3+} with Ca^{2+} and Si^{2+} implies the formation of C-A-S-H gel or partially AFm phases. Regions enriched in Cl^- are associated with the formation of Friedel's salt.

Based on these interpretations, the cement paste at 3 days (Fig. 13) displays the coexistence of C-S-H gels and CH crystals. With the incorporation of seawater during mixing, the density of C-S-H increases, attributable to the accelerated hydration process. Furthermore, the aluminum phase in WMP reacts with C-S-H to form C-A-S-H gel, contributing to a denser and more compact microstructure. The cement pastes at 7 and 28 days (Figs. 14 and 15, respectively) show no significant changes in microstructural characteristics.

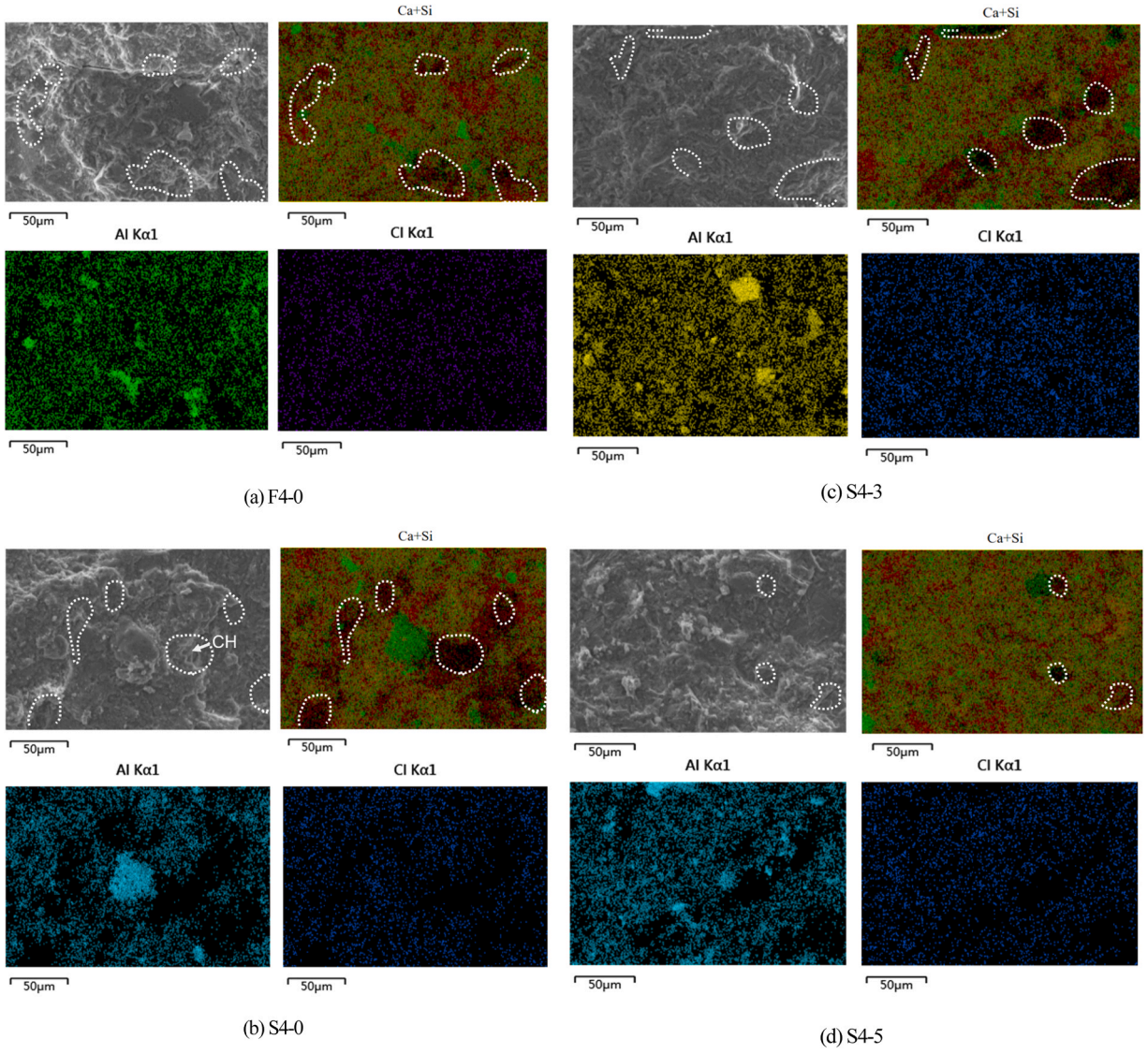

Fig. 15. Microstructure morphology at 28 days.

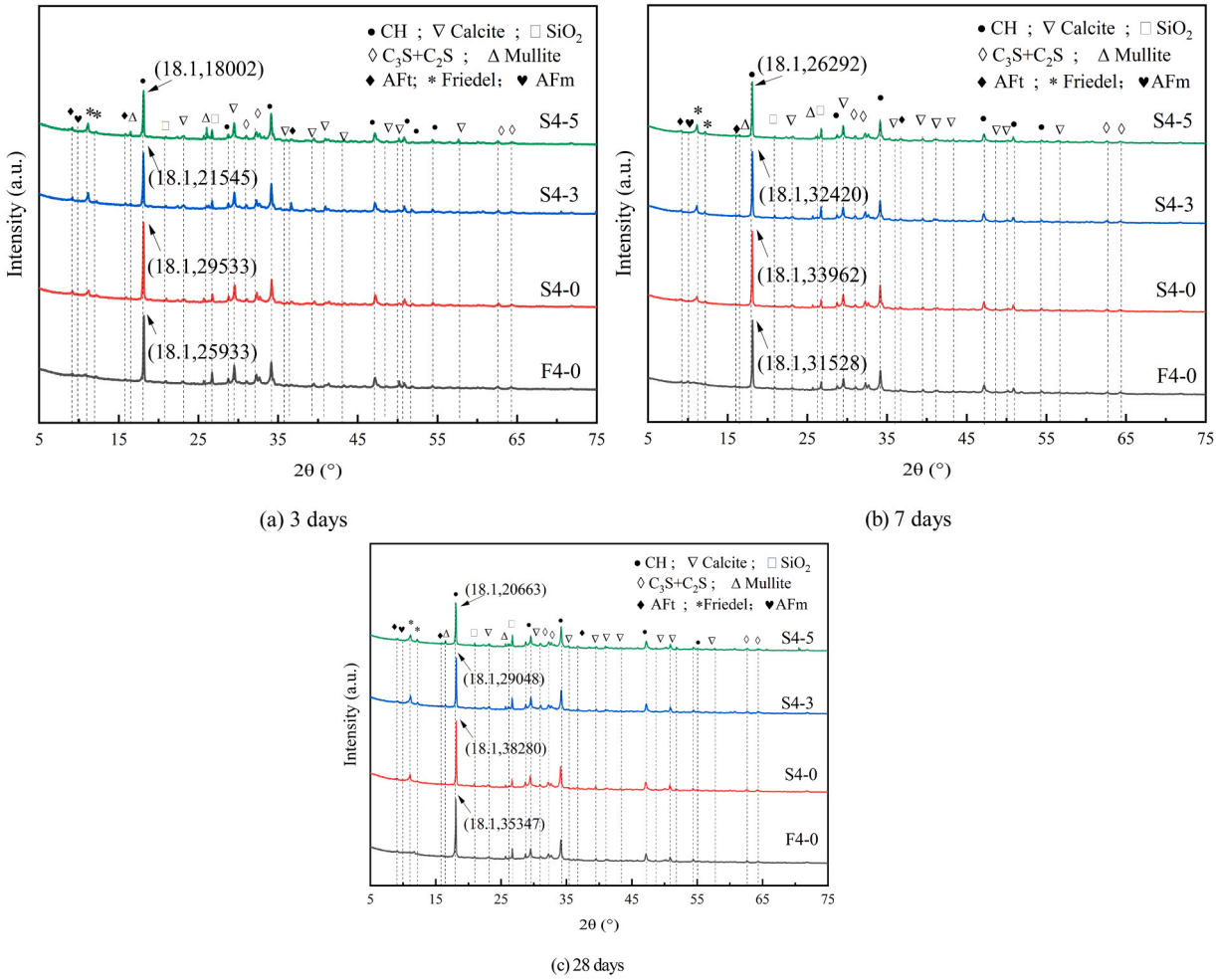

Fig. 16. XRD pattern of cement paste samples.

3.9.2. XRD

Fig. 16 presents the XRD spectra for four distinct mix proportions of freshwater-based F4–0 and seawater-based S4–0, S4–3, and S4–5, analyzed at 3, 7, and 28 days of curing. By observing the diffraction peaks, it is clear that the sample powder's primary crystalline phases resemble those found in the majority of cement paste hydration products, including CH, AFt, and unhydrated cement clinker C_3S and C_2S. Compared to freshwater mixing, the CH absorption peak intensity in SCP hydration products is markedly increased, aligning with SEM observations that suggest seawater promotes an accelerated cement hydration rate. The peak intensity corresponding to WMP gradually decreases with the increase of age, indicating that WMP is continuously consumed as hydration progresses. Additionally, the S4–3 and S4–5 groups with WMP compared to the F4–0 and S4–0 groups without WMP, not only produce hydration products from freshwater mixing but also generate AFt and Friedel's salt. This is because the aluminum phase in the WMP can absorb and solidify the free chloride ions in seawater, further illustrating that WMP can enhance the resistance of cement to seawater erosion.

The XRD spectra show the dynamic equilibrium between early-stage CH formation and Friedel's salt generation. At the early age (3 days), sea water and WMP accelerates the hydration of C_3S, resulting in CH production that exceeds its consumption by Friedel's salt formation, thereby intensifying the CH peaks. In contrast, at later ages (28 days), the increased formation of Friedel's salts and the pozzolanic reaction—confirmed by TGA—substantially consume CH. Moreover, it should be noted that XRD peak intensity is influenced by crystal size and orientation, and does not directly represent the absolute quantity of CH. These observations suggest that WMP affects CH content through a dual mechanism: promoting CH formation in the early stage, and subsequently reducing CH content through chemical binding and physical adsorption, ultimately facilitating the effective immobilization of chloride ions.

3.9.3. TGA

Fig. 17 shows the TGA results for the cement paste samples F4–0, S4–0, S4–3, and S4–5. According to Eq. (5) to Eq. (7), the calculated CH content for each mix ratio at the three ages of 3d, 7d, and 28d is shown in Fig. 18. Compared to freshwater mixing, the

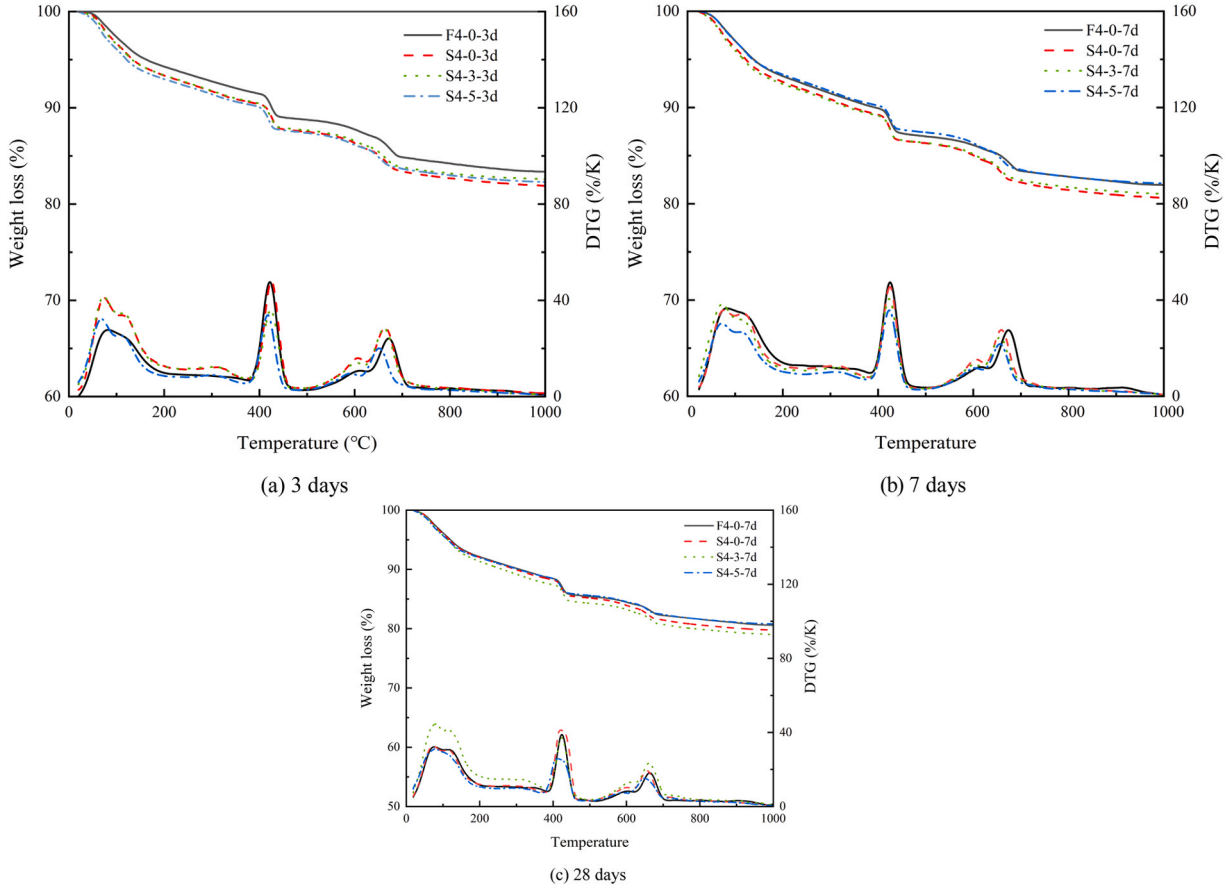

Fig. 17. TGA of cement paste samples.

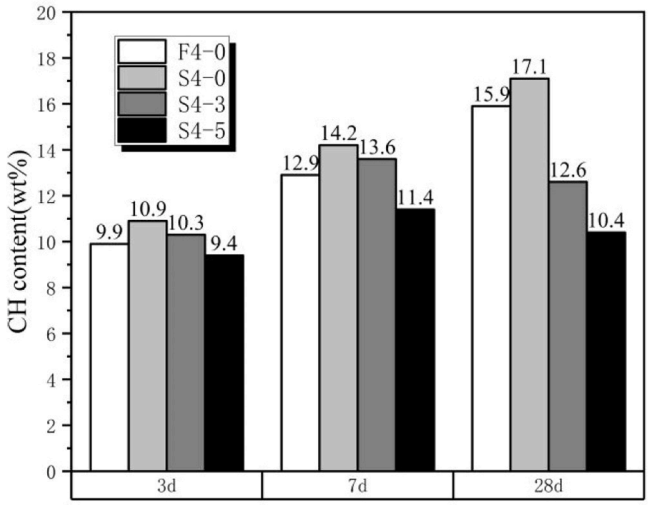

Fig. 18. Mass fraction of CH in cement paste samples.

CH content in the samples mixed with seawater significantly increases, which is in line with the SEM and XRD results. As the hydration continues, the CH in F4–0 and S4–0 shows varying degrees of increase compared to the 3d age. However, after adding WMP, within the same age period, the CH content in groups S4–3 and S4–5 shows a declining trend with higher WMP incorporation, mainly due to pozzolanic reaction between SiO_2 in WMP and cement hydration products, leading to CH consumption. Consequently, the CH content

demonstrates an initial rise followed by a gradual reduction as curing age progresses. The more WMP added, the greater the decrease in CH in the later stages, indicating that the hydration reaction is more complete.

3.9.4. FTIR

The FTIR is displayed for cement pastes with varying mix percentages in Fig. 19. At wavelengths 3640 cm^{-1}, 1650 cm^{-1}, 1420 cm^{-1}, 1084 cm^{-1}, 953 cm^{-1}, 872 cm^{-1}, and 454 cm^{-1}, a number of discrete absorption peaks are discernible. These include the narrow peaks at 872 cm^{-1} and 1420 cm^{-1}, which are caused by the vibrational contraction of the C-O-C bonds in carbonates and show that the specimens' surfaces have undergone carbonation. This is in line with the endothermic and $CaCO_3$ characteristic peaks that were seen in the XRD and TGA test findings. It is the symmetric stretching vibration of Si-O-Si bonds in amorphous silica hydrate that causes the spectral characteristic at approximately 1084 cm^{-1} . The stretching of the Si-O-Si bonds in C-S-H gel is the reason for the high absorption band at about 953 cm^{-1} . Moreover, the stretching of the Al-O-Si bonds in C-A-S-H is responsible for the peak at 709 cm^{-1} , suggesting that C-A-S-H is formed when Si^{4+} is substituted with Al^{3+} in the C-S-H structure. These spectroscopic results show that WMP promotes the conversion of silicate chains into aluminosilicate chains, strengthening the material's resistance to chloride penetration and increasing its ability to bind chloride ions.

3.9.5. The Influence of Al/Si ratio on chloride diffusion

The relationship between the Al/Si ratio and chloride ion distribution within the specimens, as determined by energy dispersive spectroscopy (EDS) analysis, is graphically represented in Fig. 20.

Experimental observations revealed a progressive reduction in chloride ion within the specimens as curing duration extended. This

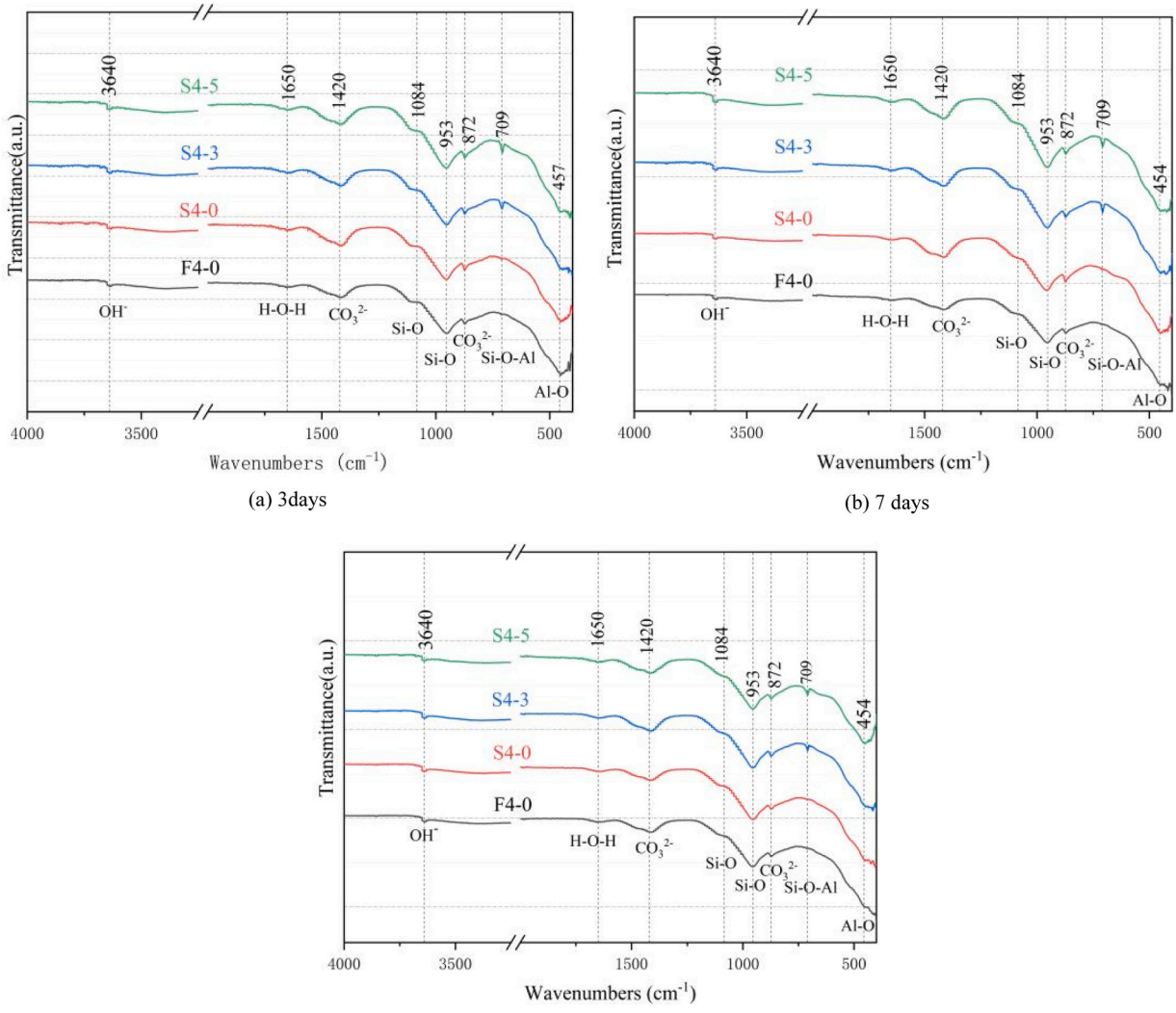

(a) 3days

(b) 7 days

(c) 28 days

Fig. 19. FTIR of cement paste samples.

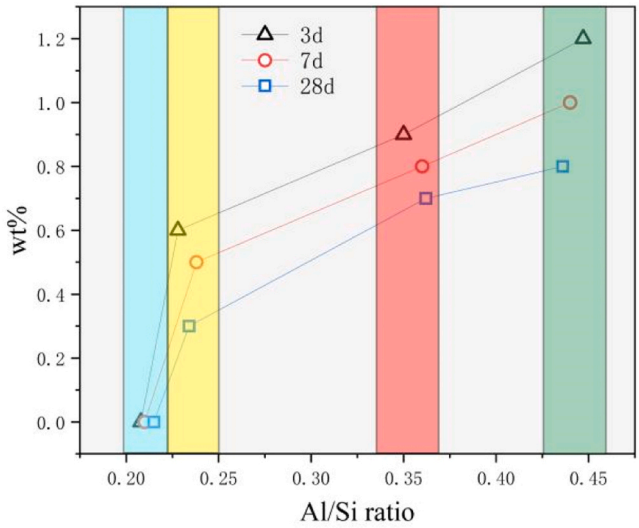

Fig. 20. Chloride binding capacity of cement pastes.

phenomenon can be explained by the freshwater curing conditions facilitating outward diffusion of chloride ions from the internal matrix, driven by concentration differentials established during the initial seawater mixing phase. Conversely, an elevation in the Al/Si ratio, achieved through WMP incorporation, resulted in increased chloride retention within the cementitious matrix. The enhancement of chloride binding capacity in cement-based systems can be primarily achieved through two distinct mechanisms: firstly, by increasing the amount of hydrated calcium aluminate phases (AFm) in the cement matrix. A higher content of AFm can absorb more chloride to form Friedel's salt and Kuzel's salt, thereby improving the chemical adsorption capacity of the cement-based system for chloride ions. Secondly, by generating C-A-S-H gel, the physical adsorption capacity of the cement-based system for chloride can be enhanced. The content of each component in the sample obtained through analysis of XRD experimental data by MDI Jade software, as shown in Fig. 21. Due to the limited effectiveness of XRD in identifying amorphous phases (C-S-H and C-A-S-H gel), the CH content derived from TGA was employed to adjust the data accordingly.

As illustrated in Fig. 21, the chloride ion content within the tested specimens demonstrates a progressive increase corresponding to higher WMP incorporation levels, indicating that the chloride diffusing from the interior to the exterior of the samples decrease. WMP contains a large amount of Al_2O_3 which combines with AFt to generate AFm. AFm then reacts with chloride in the solution to form Friedel's salt and Kuzel's salt. The phase transformation trends seen in XRD analysis for groups S4–3 and S4–5 are consistent with the chemical reaction's efficient stabilization of free chloride ions within the pore solution, characterized by a reduction in AFt phase

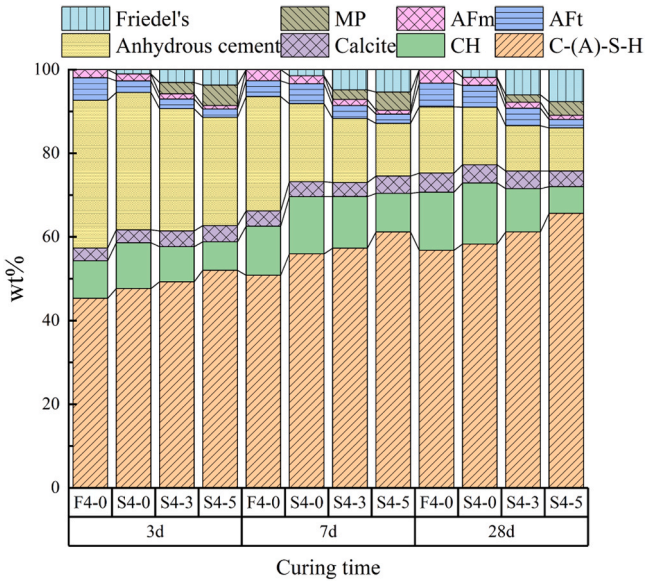

Fig. 21. phase content of cement pastes.

content accompanied by an increase in AFm phase and Friedel's salt formation.

The XRD analysis did not detect any characteristic peaks corresponding to Kuzel's salt. The increased chloride ions in the seawater simulation environment is the cause of this phenomenon, which likely promoted the conversion of Kuzel's salt to Friedel's salt through chemical interaction. The underlying reaction mechanism is illustrated in the following chemical equation:

$$3CaO \cdot Al_2O_3 \cdot 0.5CaSO_4 \cdot 0.5CaCl_2 \cdot 11H_2O + Cl^- \rightarrow 3CaO \cdot Al_2O_3 \cdot CaCl_2 \cdot 10H_2O + 0.5SO_4^{2-} + H_2O \quad (12)$$

Consequently, the amount of chemically adsorbed chloride (*Cchem*) during the hydration process can be obtained through the equation provided.

$$C_{Chem} = \omega_F \cdot n \cdot 1000 \cdot M_{Cl}/M_F \quad (13)$$

In the equation, C_{Chem} represents the chemically adsorbed amount of chloride, in *mg/g*; ω_F denotes the mass fraction of Friedel's salt; *n* indicates that each mole of Friedel's salt contains *n (n = 2)* moles of chloride ions; M_{Cl} and M_F represent the molar masses of chloride ions and Friedel's salt, respectively. The calculation results are illustrated in Fig. 22

C_{Cl}-C_{Chem} represents the chloride content in the specimen that is not chemically bound but rather consists of the sum of the chloride physically adsorbed by C-A-S-H gel and the free chloride ions present in the pores of the specimen. Under freshwater curing conditions, the free chloride ions in specimen pores and those physically adsorbed on C-A-S-H gels gradually diffused into the curing solution due to concentration gradients, resulting in decreasing chloride content over time. During the initial 3-day curing period, the C_{Cl}-C_{Chem} values of HS-3 and HS-5 groups increased from 0.54 % to 0.73 % and 1.00 % respectively, while C_{Chem} values rose from 0.06 % to 0.17 % and 0.20 %. The chemically bound chlorides contributed up to 36.7 % of the total chloride content increase. At 28 days of curing, C_{Cl}-C_{Chem} values for HS-3 and HS-5 groups further increased from 0.20 % to 0.38 % and 0.49 % respectively, with C_{Chem} values reaching 0.32 % and 0.41 %. The contribution rate of chemically bound chlorides peaked at 55 %. This indicates that the enhanced chloride immobilization capacity in WMP-modified cementitious systems during later hydration stages was primarily attributed to the formation of Friedel's salt through reactions between Al_2O_3 in WMP and chloride ions, whereas physical adsorption by C-A-S-H gels remained the dominant mechanism during early hydration stages and in WMP-free systems.

4. Conclusions

This research implemented a systematic experimental investigation to evaluate the influence of seawater and different WMP incorporation levels on the rheological properties of cementitious pastes. Subsequently, the workability and mechanical properties of mortars prepared with sea sand and standard sand were compared, with particular attention to the influence of different WMP contents. After then, the impact of WMP content on the workability and durability of SSC was examined. Finally, it was investigated how the WMP content affected the cement pastes' microstructure. The following is a summary of the primary findings from these studies:

(1) Rheological characterization demonstrated that cement pastes prepared with both seawater and freshwater exhibited Bingham fluid behavior across all tested w/c and WMP contents. Notably, as compared to their freshwater counterparts, SCP showed noticeably higher yield stress and plastic viscosity values. When WMP was added, the rheological parameters of the SCP increased, and too much WMP had a detrimental effect on the cement paste's flowability.

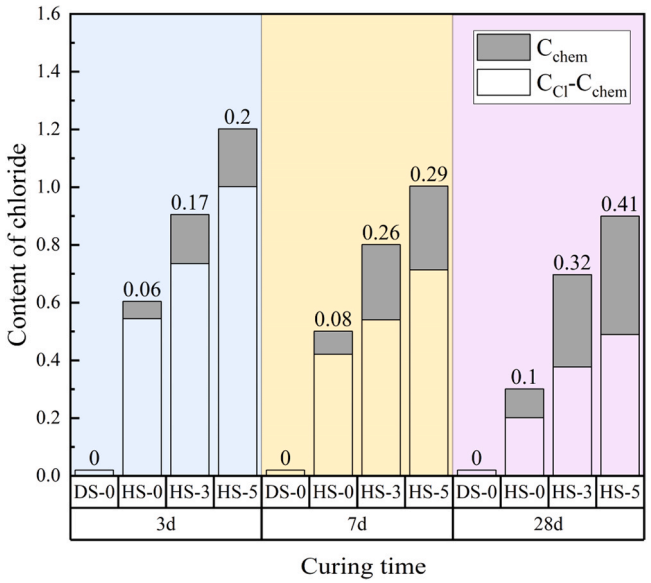

Fig. 22. Chemically Bound Chloride Content.

(2) The physical assessment of sea sand demonstrated a comparatively smaller fineness value, which translated into reduced flow capacity for corresponding mortar specimens relative to standard sand mixtures prepared at the same w/c. The investigation also revealed that elevated WMP concentrations imposed greater restrictions on the mortar's fluid behavior. At the 7 days, the compressive strength of marine sand-based mortar exhibited a marginal reduction compared to conventional sand mortar formulations, with the difference being minimal. At lower WMP contents (3 % and 5 %), optimal enhancement of mortar compressive strength was observed. Nevertheless, a strength reduction phenomenon emerged at WMP incorporation levels exceeding 10 %, it had a detrimental effect on the compressive properties.
(3) The fluidity of SSC was found to be inadequate, necessitating the addition of a certain amount of water-reducing agent to ensure its workability. The addition of WMP negatively impacted the fluidity of the concrete, meaning that the WMP content must be closely regulated. Excessive amounts of WMP would require higher dosages of superplasticizer, resulting in increased costs.
(4) Regarding sulfate corrosion resistance under dry-wet cycle conditions, during the initial phase, the compressive performance of cementitious materials exhibited a substantial improvement due to the incorporation of sulfate compounds. However, its corrosive effects became more pronounced after 60 dry-wet cycles. Studies revealed that WMP supplementation contributed to both strength development and increased resistance to sulfate corrosion in cement-based materials. A high degree of consistency was observed between the RIM analysis outcomes and the results of the electrochemical chloride permeability test, further validating the use of iodine ions as a substitute for chloride ions in evaluating the durability of SSC. The experimental evidence demonstrates WMP's effectiveness in improving the cementitious composite's barrier properties against external ionic diffusion.
(5) The incorporation of WMP leads to a denser internal structure of the cement specimens. Simultaneously, the incorporation of aluminum-containing compounds significantly enhances the hydration kinetics, leading to substantial formation of C-S-H phases and chloroaluminate complexes within the cementitious matrix. This enhancement not only improves the chloride ion immobilization capacity of the cementitious matrix through physical binding mechanisms but also substantially increases its capacity for chemical adsorption, with the latter effect being particularly pronounced.

In conclusion, the appropriate addition of WMP to SSC not only reduces the amount of cementitious material required but also enhances the performance of marine structural concrete. This technological innovation demonstrates considerable promise for facilitating the extensive implementation of self-consolidating concrete within contemporary construction practices.

CRediT authorship contribution statement

Ma hongyan: Methodology, Conceptualization. **Sun Xiao:** Writing – review & editing, Validation, Project administration, Funding acquisition, Conceptualization. **zhou zehui:** Writing – original draft, Validation, Formal analysis. **He Wenjie:** Writing – original draft, Investigation, Formal analysis. **Bi Yudong:** Investigation, Formal analysis, Data curation. **Wang Yao:** Visualization. **Liu Hengrui:** Visualization. **Zhong Rui:** Methodology.

Declaration of generative AI and AI-assisted technologies in the writing process

While preparing this work, the authors utilized ChatGPT to assist with grammar review and text refinement. After using this tool, the authors thoroughly reviewed and edited the content as necessary and assume full responsibility for the final publication.

Declaration of Competing Interest

The authors declare that they have no known competing financial interests or personal relationships that could have appeared to influence the work reported in this paper.

Acknowledgements

The financial support from the National Natural Science Foundation of China [Grant number 52279131 and 51909072].

Data availability

Data will be made available on request.

References

[1] J. Xiao, C. Qiang, A. Nanni, K. Zhang, Use of sea-sand and seawater in concrete construction: Current status and future opportunities, Constr. Build. Mater. 155 (2017) 1101–1111.
[2] UN Water, The United Nations World Water Development Report 2021: Valuing Water, UN Water, Geneva, Switzerland, 2021.
[3] UN, Comprehensive assessment of the freshwater resources of the world, UN, New York, USA, 1997.
[4] T. Dhondy, A. Remennikov, M.N. Shiekh, Benefits of using sea sand and seawater in concrete: a comprehensive review, Aust. J. Struct. Eng. 20 (4) (2019) 280–289.

[5] J.-C. Lao, B.-T. Huang, L.-Y. Xu, M. Khan, Y. Fang, J.-G. Dai, Seawater sea-sand Engineered Geopolymer Composites (EGC) with high strength and high ductility, Cem. Concr. Compos. 138 (2023) 104998.
[6] M. Etxeberria, A. Gonzalez-Corominas, P. Pardo, Influence of seawater and blast furnace cement employment on recycled aggregate concretes' properties, Constr. Build. Mater. 115 (2016) 496–505.
[7] M. Guo, B. Hu, F. Xing, X. Zhou, M. Sun, L. Sui, Y. Zhou, Characterization of the mechanical properties of eco-friendly concrete made with untreated sea sand and seawater based on statistical analysis, Constr. Build. Mater. 234 (2020) 117339.
[8] S. Kaushik, S. Islam, Suitability of sea water for mixing structural concrete exposed to a marine environment, Cem. Concr. Compos. 17 (3) (1995) 177–185.
[9] M. Etxeberria, J.M. Fernandez, J. Limeira, Secondary aggregates and seawater employment for sustainable concrete dyke blocks production: Case study, Constr. Build. Mater. 113 (2016) 586–595.
[10] A. Younis, U. Ebead, P. Suraneni, A. Nanni, Fresh and hardened properties of seawater-mixed concrete, Constr. Build. Mater. 190 (2018) 276–286.
[11] J. Limeira, L. Agulló, M. Etxeberria, Dredged marine sand as a new source for construction materials, Mater. De. ConstrucciónN. 62 (305) (2012) 7–24.
[12] B. Safi, M. Saidi, A. Daoui, A. Bellal, A. Mechekak, K. Toumi, The use of seashells as a fine aggregate (by sand substitution) in self-compacting mortar (SCM), Constr. Build. Mater. 78 (2015) 430–438.
[13] E.-I. Yang, S.-T. Yi, Y.-M. Leem, Effect of oyster shell substituted for fine aggregate on concrete characteristics: Part I. Fundamental properties, Cem. Concr. Res. 35 (11) (2005) 2175–2182.
[14] Q. Guo, L. Chen, H. Zhao, J. Admilson, W. Zhang, The effect of mixing and curing sea water on concrete strength at different ages. MATEC Web of Conferences, EDP Sciences, 2018, p. 02004.
[15] W. Zang, L. Guo, Y. Cao, J. Zhang, X. Xue, The interaction between chloride ion and sulfate ion doped in cement paste, Mater. Rep. 33 (2019) 1317–1321.
[16] T.U. Mohammed, H. Hamada, T. Yamaji, Performance of seawater-mixed concrete in the tidal environment, Cem. Concr. Res. 34 (4) (2004) 593–601.
[17] W. Jau, J. Tan, C. Yang, Effect of sea sand on concrete durability and its management, J. Southeast Univ. (Nat. Sci. Ed.) 36 (2) (2006) 161–166.
[18] Y.T. Li, L. Zhou, M. Jiang, Y. Zhang, J. Shao, Experimental study on mechanical property of concrete based on seawater and sea sand, Adv. Mater. Res. 641 (2013) 574–577.
[19] E.-I. Yang, M.-Y. Kim, H.-G. Park, S.-T. Yi, Effect of partial replacement of sand with dry oyster shell on the long-term performance of concrete, Constr. Build. Mater. 24 (5) (2010) 758–765.
[20] A. Elliott Richardson, T. Fuller, Sea shells used as partial aggregate replacement in concrete, Struct. Surv. 31 (5) (2013) 347–354.
[21] N. Thaulow, S. Sahu, Mechanism of concrete deterioration due to salt crystallization, Mater. Charact. 53 (2-4) (2004) 123–127.
[22] J. Xiao, F. Lu, Z. Sun, Study on chloride ion permeability of high performance concrete with desalted sea sand, Ind. Build. 34 (5) (2004) 4–6.
[23] Z. Jiang, T. Zhao, X. Song, Study on carbonation performance of sea sand concrete, Eng. Constr. 41 (4) (2009) 11–15.
[24] T. Yamato, Y. Emoto, M. Soeda, Freezing and thawing resistance of concrete containing chloride, Spec. Publ. 100 (1987) 901–918.
[25] E. Jones, M. Qadir, M.T. Van Vliet, V. Smakhtin, S.-m Kang, The state of desalination and brine production: A global outlook, Sci. Total Environ. 657 (2019) 1343–1356.
[26] J.-X. Zhu, K.-F. Weng, B.-T. Huang, L.-Y. Xu, J.-G. Dai, Ultra-High-Strength Engineered Cementitious Composites (UHS-ECC) panel reinforced with FRP bar/grid: Development and flexural performance, Eng. Struct. 302 (2024) 117193.
[27] D. Ramachandran, R. George, V. Vishwakarma, U. Kamachi Mudali, Strength and durability studies of fly ash concrete in sea water environments compared with normal and superplasticizer concrete, KSCE J. Civ. Eng. 21 (2017) 1282–1290.
[28] Y.-L. Li, X.-L. Zhao, R.S. Raman, S. Al-Saadi, Thermal and mechanical properties of alkali-activated slag paste, mortar and concrete utilising seawater and sea sand, Constr. Build. Mater. 159 (2018) 704–724.
[29] Z. Shi, Z. Shui, Q. Li, H. Geng, Combined effect of metakaolin and sea water on performance and microstructures of concrete, Constr. Build. Mater. 74 (2015) 57–64.
[30] M.D. Jackson, J. Moon, E. Gotti, R. Taylor, S.R. Chae, M. Kunz, A.H. Emwas, C. Meral, P. Guttmann, P. Levitz, Material and elastic properties of Al-tobermorite in ancient Roman seawater concrete, J. Am. Ceram. Soc. 96 (8) (2013) 2598–2606.
[31] R.J. Myers, E. L'Hôpital, J.L. Provis, B. Lothenbach, Effect of temperature and aluminium on calcium (alumino) silicate hydrate chemistry under equilibrium conditions, Cem. Concr. Res. 68 (2015) 83–93.
[32] Standardization Administration of PRC, Sand for construction GB/T 14684-2022, State Administration for Market Regulation, Beijing, China, 2022.
[33] Standardization Administration of PRC, Test methods for water requirement of normal consistency,setting time andsoundness of the portland cement GB/T 1346-2011, General Administration of Quality Supervision, Inspection and Quarantine, Beijing, China, 2011.
[34] State Administration for Market Regulation, Standard for test methods of concrete physical and mechanical properties GB/T 50081-2019, Ministry of Housing and Urban-Rural Development of the PRC, Beijing, China, 2019.
[35] China Building Materials Industry Association, Test method for fluidity of cement mortar GB/T 2419-2005, China National Standardization Administration Committee, Beijing, China, 2005.
[36] BIBM, CEMBUREAU, ERMCO, EFCA, EFNARC, The European guidelines for self-compacting concrete, Farnham, UK, EFNARC, 2005, p. 563.
[37] X. Sun, H. Liu, Z. Tian, Y. Ma, Z. Wang, H. Fan, Feasibility and economic evaluation of grouting materials containing binary and ternary industrial waste, Constr. Build. Mater. 274 (2021) 122021.
[38] A. Kwan, J. Chen, Adding fly ash microsphere to improve packing density, flowability and strength of cement paste, Powder Technol. 234 (2013) 19–25.
[39] China Academy of Building Research, Standard for test methods of long-term performance and durability of ordinary concrete GB/T 50082-2009, Ministry of Housing and Urban-Rural Development of the PRC, Beijing, China, 2009.
[40] Y. Wang, K. Fu, Comparisons of instantaneous chloride diffusion coefficients determined by RCM method and chloride natural diffusion test, Constr. Build. Mater. 223 (2019) 595–604.
[41] H. Weilin, M. Zhiming, Z. Tiejun, L. Feng, Study on the Mechanism of Sulphate Erosion of Concrete in Marine Environment, China Concr. Cem. Prod. 000 (007) (2014) 17–20.
[42] J. Limeir, L. Agulló, M. Etxeberria, Dredged marine sand as construction material, Eur. J. Environ. Civ. Eng. 16 (8) (2012) 906–918.
[43] W. Hou, J. Liu, Z. Liu, F. He, J. Zhu, Y. Cui, W. Jinyang, Calcium transfer process of cement paste for ettringite formation under different sulfate concentrations, Constr. Build. Mater. 348 (2022) 128706.
[44] X. Liu, P. Feng, X. Yu, J. Huang, Decalcification of calcium silicate hydrate (CSH) under aggressive solution attack, Constr. Build. Mater. 342 (2022) 127988.
[45] W. Kunther, B. Lothenbach, J. Skibsted, Influence of the Ca/Si ratio of the C–S–H phase on the interaction with sulfate ions and its impact on the ettringite crystallization pressure, Cem. Concr. Res. 69 (2015) 37–49.
[46] L. Wang, Z. He, B. Zhang, X. Cai, Polymerization mechanism of CSH: identified by FTIR and NMR, J. Build. Mater. 14 (4) (2011) 447–451.
[47] M.D. Jackson, S.R. Chae, S.R. Mulcahy, C. Meral, R. Taylor, P. Li, A.-H. Emwas, J. Moon, S. Yoon, G. Vola, Unlocking the secrets of Al-tobermorite in Roman seawater concrete, Am. Mineral. 98 (10) (2013) 1669–1687.
[48] B.-T. Huang, J.-Q. Wu, J. Yu, J.-G. Dai, C.K. Leung, V.C. Li, Seawater sea-sand engineered/strain-hardening cementitious composites (ECC/SHCC): assessment and modeling of crack characteristics, Cem. Concr. Res. 140 (2021) 106292.